IVYSPRING INTERNATIONAL PUBLISHER

Theranostics

2025; 15(16): 8012-8030. doi: 10.7150/thno.112781

Review

Imaging hypoxia for head and neck cancer: current status, challenges, and prospects

Wenhui Huang[1,2,3*], Nemin Li[1*], Sheng Zhu[4*], Yuze Zhang[1], Xinyang Song[1], Bin Zhang[1], Hao Yan[5], Jie Tian[6]✉, Kun Wang[3]✉, Shuixing Zhang[1,2]✉

1. State Key Laboratory of Bioactive Molecules and Druggability Assessment, the First Affiliated Hospital, Jinan University, Guangzhou, 510632, China.
2. Guangdong Basic Research Center of Excellence for Natural Bioactive Molecules and Discovery of Innovative Drugs, College of Medicine, Jinan University, Guangzhou, 510632, China.
3. CAS Key Laboratory of Molecular Imaging, the State Key Laboratory of Management and Control for Complex Systems, Institute of Automation, Chinese Academy of Sciences, Beijing, 100190, China.
4. Department of Nuclear Medicine, the Affiliated Hospital of Xiangnan University, Chenzhou, 423000, China.
5. Tsinghua Shenzhen International Graduate School, Tsinghua University, Shenzhen, 518055, China.
6. Beijing Advanced Innovation Center for Big Data-Based Precision Medicine, School of Engineering Medicine, Beihang University, Beijing, 100191, China.

*Co-first authors.

✉ Corresponding authors: Shuixing Zhang, College of Medicine, Jinan University, No. 163, Huangpu West Road, Tianhe District, Guangzhou, 510632, China; Email: zsx7515@jnu.edu.cn. Kun Wang, CAS Key Laboratory of Molecular Imaging, the State Key Laboratory of Management and Control for Complex Systems, Institute of Automation, Chinese Academy of Sciences, No. 95 Zhongguancun East Road, Haidian District, Beijing, 100190, China; E-mail: kun.wang@ia.ac.cn. Jie Tian, Beijing Advanced Innovation Center for Big Data-Based Precision Medicine, School of Engineering Medicine, Beihang University, Beijing, 100191, China; Email: jie.tian@ia.ac.cn.

Received: 2025.02.25; Accepted: 2025.06.30; Published: 2025.07.11

Abstract

Hypoxia can substantially impact clinical outcomes in patients with head and neck cancer (HNC) by promoting tumor invasion, metastasis, immune escape, and therapy resistance. Given the growing interest in targeting hypoxia for cancer therapy, noninvasive methods are needed to accurately detect hypoxia and evaluate the tumor response to treatment. This review summarizes recent advances in hypoxia-targeted probes and imaging techniques, emphasizing their imaging mechanisms, strengths, and limitations. We focused on the promising clinical applications of hypoxia imaging, especially those currently used in clinics, such as positron emission tomography and magnetic resonance imaging, and highlighted their roles in guiding personalized therapy. Future directions include optimizing imaging probes to improve safety profiles, integrating multimodal imaging, applying machine learning models to analyze multiparametric data, and establishing standardized 3-dimensional *in vitro* models to better mimic hypoxia heterogeneity. These advancements are expected to considerably improve the management of patients with HNC.

Keywords: tumor hypoxia, head and neck cancers, positron emission tomography, magnetic resonance imaging, optical molecular imaging

1. Introduction

Head and neck cancer (HNC) arises from the mucosal epithelium of the oral cavity, pharynx, and larynx, and over 90% of these tumors are classified as squamous cell carcinoma [1]. Existing screening strategies are known to be less effective in detecting early stages of HNCs, and physical examination remains the mainstay approach for early detection [2]. Treatment for HNCs involves surgery and radiochemotherapy, depending on the disease stage and tumor type. Despite advances in diagnosis and treatment, prognostic outcomes vary among patients after treatment. Hypoxia, known to arise from an imbalance between oxygen (O_2) demand and delivery within tumor tissues, has been identified as a key factor contributing to tumor aggressiveness and treatment resistance [3]. Hypoxia is a key characteristic of solid tumors, making it a crucial target for imaging and treatment [4]. Recent studies have profiled hypoxia-regulated gene expression in more than 9,000 individual tumors and have determined that HNCs exhibit some of the highest hypoxic gene expression scores [5]. Extensive evidence has revealed that hypoxia affects radiotherapy outcomes by activating DNA repair mechanisms and altering cellular signaling pathways, leading to the failure of radiation-induced cytotoxicity

[4, 6]. Accordingly, hypoxia imaging plays a dominant role in optimizing treatment strategies and improving outcomes in patients with HNC.

Advances in imaging technology have enabled the detection and visualization of tumor hypoxia. Positron emission tomography (PET)/computed tomography (CT) imaging with hypoxia-targeted radiotracers such as [^{18}F] fluoroazomycin arabinoside (^{18}F-FAZA) and [^{18}F] flortanidazole (^{18}F-HX4) has shown promise for spatially mapping hypoxic regions in tumors [7]. Magnetic resonance imaging (MRI) with or without oxygen-sensitive contrast agents offers a high spatial resolution. Additionally, optical molecular imaging (OMI) modalities, including fluorescence, phosphorescence, photoacoustic, and Cherenkov imaging, are being explored for the real-time detection of cyclic hypoxia [8]. In addition to the considerable progress in imaging techniques, advances in bioimaging technology have further improved the targeting efficiency [9]. With the growing interest in exploiting tumor hypoxia as a therapeutic target [10,11], hypoxia imaging has broad application prospects, such as guiding radiotherapy or immunotherapy, tracking tumor metastases *in vivo*, and screening hypoxia-activated prodrugs (HAPs) [12]. This review provides a concise overview of the design strategies for hypoxia probes, with a primary focus on advances in imaging technologies and their promising applications in patients with HNC (**Graphical Abstract**).

2. Design Strategies for Hypoxia-Targeted Probes

The development of functional molecules and nanoparticles for hypoxia imaging enables *in vivo* monitoring of biological processes and disease states. Typically, when oxygen levels fall below 3%, the expression of hypoxia-induced factor-1alpha (HIF-1α) is upregulated, subsequently activating downstream signaling pathways critical for cellular survival. This process drives the production of hypoxia-associated enzymes and metabolites. Therefore, design strategies for hypoxia probes focus on detecting hypoxia-related analytes, which are categorized into physical, biological, and chemical subtypes (**Table 1**).

Direct measurement of partial oxygen pressure (pO_2) is the most straightforward approach for assessing tumor hypoxia. Invasive oxygen microelectrodes allow clinicians to measure localized tissue oxygen concentrations at specific time points, with *in vivo* noninvasive oxygen sensors increasingly favored. These sensors often utilize phosphorescent metal complexes with long-lived emissions in which oxygen molecules quench the luminescence [13,14]. Although this oxygen-induced quenching effect enables the real-time mapping of cyclic hypoxia, traditional phosphorescence-based hypoxia probes are limited to the visible and first near-infrared (NIR) wavelength regions (NIR-I, 700–900 nm), resulting in high light scattering and low penetration depth. Recent advancements have focused on developing novel organometallic complex nanoparticles for second NIR wavelength (NIR-II, 1000–1700 nm) imaging to improve the signal-to-noise ratio (SNR) and enhance tumor accumulation [15]. However, poor biocompatibility and limited tissue penetration remain the greatest obstacles to their clinical application.

Table 1. Design strategies for hypoxia-targeted probes.

Categories	Mechanism	Representative Probes	Imaging Devices	Advantages	Disadvantages	Recent Innovations	References
Physical	Direct oxygen sensing via luminescence quenching	PpyPt NPs, PtTFPP/PtOEP, Rhenium-diimine complex, Ir-BTPHSA complex, Ir-PVP, RHyLI, PtG4	PLI, CLI	Real-time Quantitative Available to detect cyclic hypoxia	Poor biocompatibility Low penetration depth Visible/NIR-I only	NIR-II probes Upconversion nanoparticles	[13,14,15,72,73,74,85]
Biological	Enzyme-activated (NTRs, AzoRs) or Receptor-targeted (CAIX)	HDSF, X4, CNO, 3-azo-conjugated BODIPY, Hypoxia-targeted radiotracers (^{18}F-FMISO,^{18}F-FAZA,^{18}F-HX4), CAIX-800, ^{99m}Tc-PHC-102	FMI, PAI, PET/CT, SPECT	High specificity Good stability Easy accessibility	Off-target activation Limited sensitivity	Multimodal strategies	[16,17,18,19,38,42,43,68,69,70,71,106]
Chemical	Detection of hypoxia-relevant chemical compounds (pH, H_2O_2, H_2S)	Ir-D, Au@Pt−Se NPs, CD-950, MB-m-borate, QN-Naph, DNNC, AGNPs, Ir-NP, SiRho-SHD-NTR, Ir-BTPHSA	FMI, PAI, PLI	High sensitivity Good specificity High SNR Real-time and rapid response	Cross-reactivity Complex synthesis Low penetration depth	Dual-lock probes Ratiometric imaging Self-calibrated probe platforms	[24,25,26,27,29,30,31,32,67,72]

NIR: near-infrared; CAIX: carbonic anhydrase IX; NTRs: nitroreductases; AzoRs: azoreductases; PLI: phosphorescence lifetime imaging; CLI: Cherenkov luminescence imaging; PAI: photoacoustic imaging; FMI: fluorescent molecular imaging; H_2O_2: hydrogen peroxide; H_2S: hydrogen sulfide; ^{18}F-FMISO: ^{18}F-Fluoromisonidazole; ^{18}F-FAZA: ^{18}F-fluoroazomycin arabinoside; ^{18}F-HX4: ^{18}F-flortanidazole; PET/CT: positron emission tomography/computed tomography; SPECT: single photon emission computed tomography; SNR: signal-to-background ratio.

Reductive species such as nitroreductases (NTRs) and azoreductases (AzoRs) accumulate in the hypoxic tumor microenvironment [16]. Hypoxia-sensitive probes that leverage nitroaromatic or azobenzene derivatives have been developed to detect redox dynamics [16-20]. These moieties, which are widely used in optical and radionuclide imaging, undergo reduction processes that directly reflect the severity of hypoxia. In addition to redox-active molecules, hypoxia-induced upregulation of carbonic anhydrase IX (CAIX), a component of the complex response of cancer cells to an evolving low-oxygen environment, is a promising target for tumor hypoxia [21]. Probes targeting CAIX typically combine ligand-receptor binding domains with signal-generating groups, offering a one-step synthesis and easy accessibility [22]. Such strategies are commonly used in preclinical and clinical studies to provide a stable and indirect method for identifying hypoxic conditions and have considerable potential for clinical translation [23].

Hypoxia-driven anaerobic glycolysis in tumors generates lactic acid, leading to extracellular acidosis (pH 6.5–6.9). To improve the accuracy of hypoxia detection, dual-sensing probes have been engineered to concurrently measure pO_2 and extracellular pH [24]. Chemical analytes linked to hypoxic signaling pathways, such as hydrogen peroxide (H_2O_2) [25] and hydrogen sulfide (H_2S) [26], are emerging targets. These hypoxia-activated probes often incorporate three components: analyte-specific sensing moieties, signal transduction systems for generating detectable outputs, and bio-orthogonal functionalization for minimizing cross-reactivity. Although these probes achieve high sensitivity and rapid response, they usually require a relatively complex synthesis process, and their potential cross-reactivity with other reactive oxygen species groups compromises their specificity.

Recent progress in designing highly selective and sensitive imaging probes for tumor hypoxia has focused on the development of dual-lock fluorescent probes and dual-emissive ratiometric probes, representing a critical step toward the next generation of smart probes [27-32]. Dual-lock fluorescent probes can markedly enhance detection specificity by requiring simultaneous activation with two hypoxia-associated biomarkers. These probes integrate naphthalimide fluorophores with hypoxia-sensitive moieties and dual-quenching mechanisms to achieve superior SNR, enabling noninvasive real-time monitoring of hypoxia [29,30]. Dual-emissive ratiometric oxygen probes offer built-in self-calibration signal correction by integrating oxygen-sensitive fluorophores with oxygen-insensitive reference materials, enabling quantitative and reliable detection of hypoxia [31,32]. This self-referencing mechanism enhances both the accuracy and reproducibility of signal acquisition, demonstrating its utility in mapping oxygen saturation ($_SO_2$) with spatial resolution and its compatibility with multimodal imaging platforms in preclinical studies. Moreover, advances in multimodal imaging devices have greatly facilitated the progress of hypoxia probes, with the combined advantages of different imaging modalities promising comprehensive and precise hypoxia quantification. The following sections discuss individual imaging modalities for tumor hypoxia (**Table 2**), their imaging tracers, and their applications in HNCs.

3. Imaging Modalities

3.1 PET

PET is an important tool for detecting tumor hypoxia because it utilizes radiotracers that target hypoxia-specific molecules [33]. These tracers, which are frequently based on the reductive tendency of nitroimidazoles, are selectively metabolized and trapped in hypoxic regions. The selection of representative ^{18}F-labeled 2-nitroimidazoles for hypoxic imaging is shown in **Figure 1A** [34]. [^{18}F] fluoromisonidazole (^{18}F-FMISO) and ^{18}F-FAZA are well-investigated first- and second-generation hypoxia PET tracers used in preclinical and clinical settings [35]. They exploit differences in oxygen levels between hypoxic and well-oxygenated tissues. When administered intravenously, they diffuse into cells, re-oxidize, and undergo clearance in well-oxygenated regions but are reduced to macromolecules and retained in hypoxic cells.

3.1.1 First-generation radiotracer: ^{18}F-FMISO

^{18}F-FMISO has been widely explored for detecting hypoxia across various tumor types, demonstrating a substantial correlation between FMISO uptake and HIF-1α expression and tissue perfusion [36]. ^{18}F-FMISO-based PET is a promising method for quantifying hypoxia, predicting patient prognosis, and optimizing treatment planning. A meta-analysis of 323 patients with HNC from 17 different studies using hypoxic PET revealed a notable positive correlation between primary tumor volume and hypoxic tracer uptake [37]. The uptake value from FMISO-based PET was identified as a prognostic indicator, indicating a worse prognosis in patients who had a high hypoxic volume on baseline images than those with a low hypoxic volume [38]. In 23 patients with oral squamous cell carcinoma, the preoperative hypoxic volume, as measured on

FMISO-based PET, correlated with disease-free survival and local recurrence [39]. However, the results of different clinical trials remain inconsistent. For example, Löck *et al.* found weak correlations between FMISO-based PET parameters and hypoxia-associated gene expression [40]. Notably, FMISO-based PET is a low-contrast imaging modality owing to its lipophilic property, with a tumor-background ratio (TBR) of 1.4–1.6, which complicates the interpretation of PET images.

3.1.2 Other nitroimidazole-based radiotracers

A new generation of hypoxia radiotracers has evolved from nitroimidazole-based compounds such as etanidazole (EF3 and EF5). Although these agents exhibit higher lipophilicity than ^{18}F-FMISO, along with easy tissue penetration and short injection-to-imaging time, their slow clearance from normoxic tissues results in a suboptimal TBR [41]. Second-generation tracers, such as ^{18}F-FAZA, address this limitation by enhancing hydrophilicity, achieving faster clearance from non-hypoxic regions, and improving the TBR [42]. Further advancements have focused on enhancing hydrophilicity to reduce nonspecific retention, generating third-generation agents with rapid renal clearance, such as ^{18}F-HX4, which has shown a 6-fold and 3-fold better TBR than ^{18}F-FMISO and ^{18}F-FAZA, respectively [43]. Currently, ^{18}F-FAZA and ^{18}F-HX4 are being extensively explored in clinical studies. In a study involving 23 patients with HNC, FAZA uptake correlated with disease progression [44]. A prospective study involving 38 patients with non-metastatic HNC (**Figure 1B-F**) revealed that higher uptake on FAZA-based PET correlated with a higher risk of local recurrence after an 8-year follow-up period [45]. For ^{18}F-HX4, a multicenter study confirmed the reproducibility in hypoxia quantification, with scan parameters revealing robust intersession correlations [46]. Additionally, HX4 uptake was substantially correlated with pimonidazole and CAIX expression, validating its biological relevance [47]. These advancements highlight the translational potential of next-generation radiotracers for refining hypoxia-driven therapeutic strategies for HNC.

Table 2. Advantages and limitations of hypoxia imaging modalities.

Techniques	Labels	Signal measured	Advantages	Limitations	Cost	Throughput	Resolution	References
PET	Radiotracers	Positrons from radionuclides	High sensitivity and specificity	Radioactive Limited spatial resolution Low SNR	High	Low	5–7 mm	[33-48]
BOLD-MRI	Label-free	Magnetic field alterations	Noninvasive Label-free High spatial resolution	Low sensitivity and specificity Susceptible to physiological factors Time-consuming scans	High	Low	1–2 mm	[50-54]
OE-MRI	Label-free	Magnetic field alterations	Noninvasive Label-free High spatial resolution	Low sensitivity Limited specificity Time-consuming scans	High	Low	1–2 mm	[54-59]
DCE-MRI	Gadolinium-based contrast agents	Vascular perfusion/permeability	High spatial resolution	Low sensitivity and specificity Time-consuming scans Require multiparametric analysis	High	Low	1–2 mm	[60-62]
FMI	Fluorescent probes	Light	No radiation Low cost Live monitoring High sensitivity	Invasiveness, Limited tissue penetration	Low	High	2–3 mm	[16-19,24,25,27-32,63,64,71,106]
PLI	Oxygen-sensitive luminescent probes	Light	No radiation, Direct oxygen levels quantification	Invasiveness Probe safety Complex imaging system Limited tissue penetration	Low	High	3–5 mm	[13-15,72-74]
PAI	Label-free or Probes	Sound	Noninvasive High spatial-temporal resolutions Deep tissue penetration	Probe safety	Low	High	1 mm	[26,67,75-82]
CLI	Label-free or Oxyphros probes	Cherenkov photons	Live monitoring High sensitivity	Radioactive Limited tissue penetration	Low	High	3–5 mm	[83-87]

PET: positron emission tomography; BOLD-MRI: blood oxygen level-dependent magnetic resonance imaging; OE-MRI: oxygen-enhanced magnetic resonance imaging; DCE-MRI: dynamic contrast enhancement magnetic resonance imaging; FMI: fluorescent molecular imaging; PLI: phosphorescence lifetime imaging; PAI: photoacoustic imaging; CLI: Cherenkov luminescence imaging.

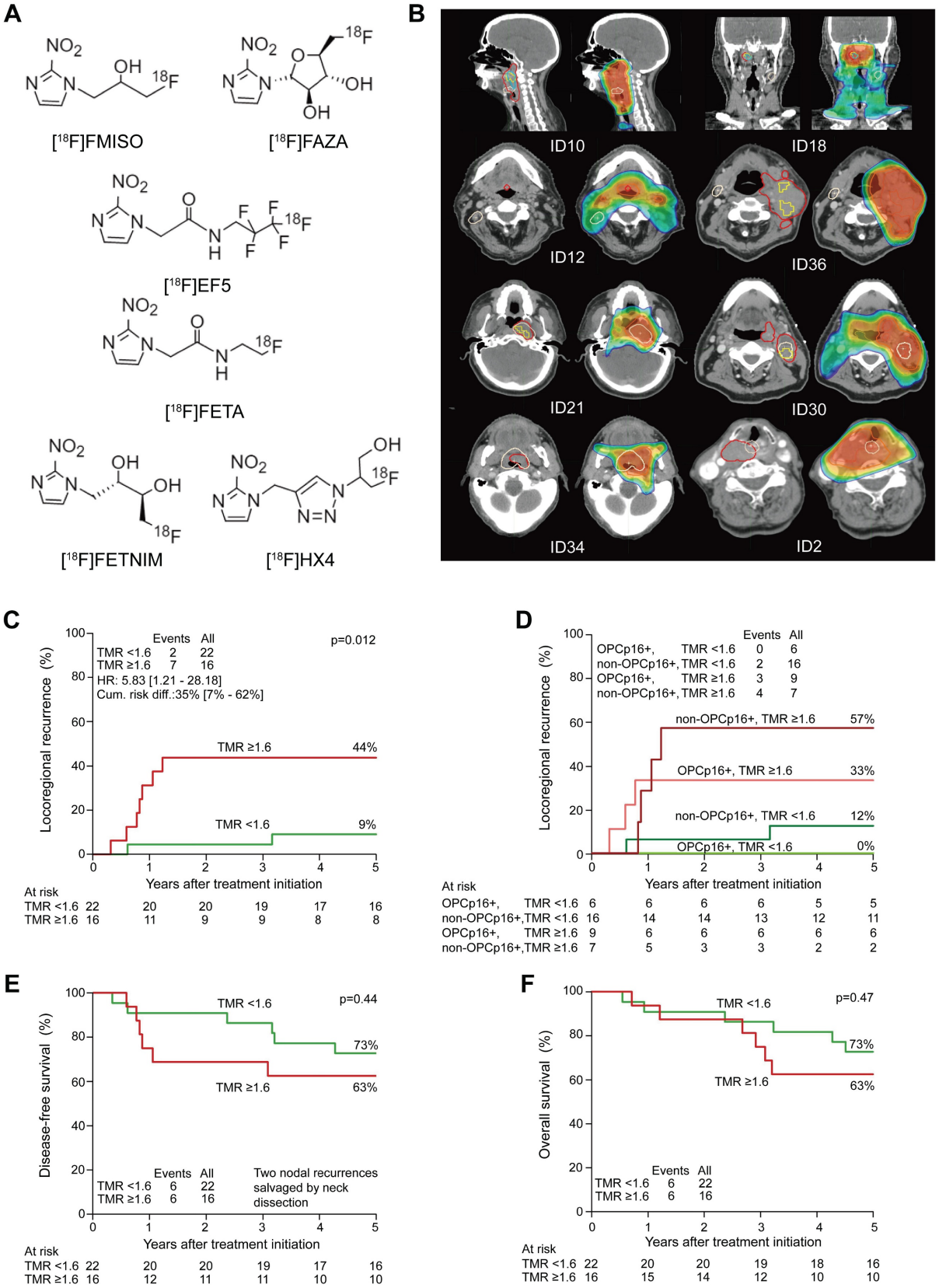

Figure 1. (A) Chemical structures of selected ^{18}F-labeled 2-nitroimidazoles used in PET imaging of tumor hypoxia. Adapted with permission from [34], an open access article under a CC-BY 4.0 license, copyright 2022 Springer Nature. (B) Hypoxic subvolumes and recurrence patterns within the primary GTV (two left rows) and dose coverage (two right rows) from the radiotherapy plan. White contours and "+" symbols mark the center of recurrent tumors. Red: GTV; yellow: hypoxic subvolumes; light blue: persistent hypoxia. (C-F) Five-year outcomes comparing more vs. less hypoxic tumors. Adapted with permission from [45], copyright 2020 Elsevier. GTV: gross tumor volume; TMR: tumor-to-muscle ratio; PET: positron emission tomography.

Although emerging evidence underscores the clinical potential of hypoxia-targeted radiotracers, notable challenges remain to be addressed. PET imaging, despite its functionality, is constrained by its limited spatial resolution (5–7 mm) and inherently low soft-tissue contrast. Tumor hypoxia exhibits spatial heterogeneity and dynamic temporal evolution, making it difficult to accurately capture hypoxic regions using a single PET scan [48]. This is particularly relevant in hypoxia image-guided radiotherapy, in which hypoxic regions need to be precisely delineated. Furthermore, conventional hypoxic radiotracers, such as ^{18}F-FMISO, suffer from prolonged uptake kinetics, necessitating delayed imaging (120–180 min post-administration), resulting in a suboptimal SNR. Advanced pharmacokinetic modeling techniques are leveraged to differentiate true hypoxia-specific tracer uptake from nonspecific background signals, thereby improving quantitative accuracy.

3.2 MRI

MRI utilizes robust magnetic fields and radiofrequency pulses to generate high-resolution functional images [49]. MRI primarily employs two contrasting mechanisms to assess hypoxia. One method uses paramagnetic contrast agents that shorten T1 relaxation times and enhance the signal intensity on T1-weighted images. The other relies on oxygen-sensitive imaging sequences such as blood oxygen level-dependent (BOLD) and oxygen-enhanced MRI, which detect endogenous signal variations linked to tissue oxygenation levels. In the subsequent sub-sections, we review the principles, clinical advantages, and limitations of each method in the context of hypoxia imaging.

3.2.1 BOLD-MRI

Paramagnetic deoxyhemoglobin increases the transverse relaxation rate (R2*, defined as 1/T2*) of water protons in blood and tumor tissues, forming the basis for oxygenation-sensitive imaging via BOLD-MRI [50]. Tumor R2* decreases with elevated blood $_{S}O_2$ levels during hyperoxic gas inhalation, enabling BOLD sequences to detect oxygenation changes with high sensitivity. However, the relationship between R2* and direct tissue pO_2 measurements remains controversial. Preclinical studies have reported statistically significant associations between tumor R2* and tissue pO_2 levels [51], whereas clinical trials, including a 10-patient cohort analysis, failed to detect a significant correlation [52]. Although R2* values were found to positively correlate with HIF-1α expression or pimonidazole staining in several studies [53], the observed signal changes were subtle and markedly susceptible to O_2 changes in large vessels and surrounding tissues, hindering their ability to detect regional hypoxia. Furthermore, BOLD imaging sequences are inherently sensitive to motion artifacts and magnetic susceptibility at air-tissue interfaces, complicating their application in HNC. These technical and biological constraints underscore the need for complementary methods to assess hypoxia and validate the BOLD-derived findings in clinical settings.

3.2.2 Oxygen-enhanced MRI (OE-MRI)

OE-MRI is an emerging technique that measures free oxygen in plasma and interstitial fluid to evaluate tissue oxygenation [54]. Molecular oxygen is paramagnetic, and the longitudinal relaxation rate (R1 = 1/T1) increases linearly with increasing O_2 concentrations. In well-oxygenated tumors, elevated dissolved O_2 shortens T1, resulting in positive proton signal changes (ΔR1) similar to those observed in healthy tissues. Positive ΔR1 indicates efficient O_2 delivery, while negative ΔR1 identifies hypoxic regions. OE-MRI provides direct insights into tumor hypoxia and has garnered considerable research interest. Notably, O'Connor *et al.* introduced the concept of "perfused Oxy-R," regions with intact perfusion but absent oxygen enhancement, to distinguish hypoxic from well-oxygenated regions in preclinical models [55]. A subsequent first-in-human study demonstrated the feasibility and repeatability of OE-MRI, revealing that perfused Oxy-R could stratify patients based on post-radiotherapy hypoxia modulation, highlighting its utility in monitoring treatment responses and identifying non-responders [56]. Recently, OE-MRI was successfully transformed into volumetric and dynamic hypoxia imaging on an MRI and linear accelerator (MR-Linac) in a cohort of 15 healthy participants and 14 patients with HNC [57], achieving a 98% success rate (50/51 scans), thereby indicating its potential for clinical use in hypoxia image-guided radiotherapy.

Likewise, OE-MRI is subject to translational challenges. Key challenges include obtaining optimal acquisition timing and susceptibility artifacts at air-tissue interfaces [58,59]. Standardizing MRI protocols is critical for accurate ΔR1 quantification. Additionally, advanced computational methods such as data-driven clustering algorithms may improve hypoxia segmentation and artifact correction. Addressing these barriers is crucial for advancing OE-MRI from experimental validation to routine clinical workflows.

3.2.3 Dynamic contrast-enhanced MRI (DCE-MRI)

In tumors, hypoxic regions exhibit reduced blood flow and vascular permeability, resulting in slower clearance of contrast agents than well-oxygenated regions. DCE-MRI uses rapid sequential imaging to track the kinetics of gadolinium-based contrast agents, thereby providing indirect insights into tissue perfusion and oxygen delivery. By utilizing tracer kinetic modeling of serial MRI acquisitions, DCE-MRI quantifies microvascular parameters such as the volume transfer constant (K^{trans}), reflux rate (K_{ep}), and extracellular volume fraction (V_e). Although early studies reported weak correlations between these parameters and direct hypoxia markers, such as pimonidazole staining [60], Gaustad *et al.* demonstrated that K^{trans}, derived from pharmacokinetic modeling incorporating arterial input functions, showed a substantial correlation with tumor hypoxia in animal models [61]. DCE-MRI parameters have shown utility in detecting baseline and treatment-induced hypoxia, as well as in predicting hypoxia-induced radiation response and metastatic potential. However, it is crucial to note that DCE-MRI does not directly measure O_2 levels, necessitating integration with additional imaging modalities or molecular biomarkers for a comprehensive assessment [62]. Future efforts should focus on standardizing acquisition protocols, open data sharing, and large-scale multicenter validation studies to establish robust hypoxia-specific imaging biomarkers.

In summary, PET and MRI have demonstrated promising clinical results for detecting tumor hypoxia. However, their widespread application is constrained by high costs, time-consuming scans, and reliance on ionizing radiation or strong magnetic fields. These unmet clinical requirements have led to advancements in OMI.

4. OMI

Optical imaging enables the visualization and quantification of biological processes at the molecular level, offers high practicality and cost-friendliness, and is emerging as a fundamental tool for imaging tumor hypoxia in the field of basic science [8]. Diverse optical techniques, including fluorescence, phosphorescence, photoacoustic, and Cherenkov imaging, employ hypoxia-specific probes and advanced imaging systems to visualize and quantify hypoxic regions within tumors (**Figure 2**).

4.1 Fluorescence imaging

Fluorescence imaging is considered the most sensitive and widely used optical method for detecting hypoxia using two typical strategies: hypoxia-responsive activation and hypoxia-specific accumulation [63].

4.1.1 Hypoxia-responsive activation

These fluorescent probes function as O_2 sensors, enabling stimuli-specific "off-on" activation to enhance SNR within hypoxic regions. They typically contain hypoxia-responsive enzymes or molecules that modulate fluorescence intensity or spectral characteristics in response to hypoxic regions. Two common methods used to design such probes include aggregation-caused quenching (ACQ) and fluorescence resonance energy transfer (FRET) [64]. ACQ occurs when fluorophores in close proximity undergo energy transfer, leading to fluorescence quenching. When encapsulated tightly within nanocarriers equipped with reductive enzymes, such as azobenzene derivatives [65] or nitroreductases [66], fluorescence is selectively activated in hypoxic regions owing to carrier disassembly. The coupled FRET pairs are linked via hypoxia-cleavable groups. Under low-oxygen conditions, FRET occurs when a donor fluorophore transfers energy to a receptor fluorophore through non-radiative mechanisms, furnishing a direct response to targeted analytes with improved specificity and SNR [67]. Although ACQ and FRET probes are well-established in preclinical imaging, their applications in patients with HNC remain unexplored.

4.1.2 Hypoxia-specific accumulation

Hypoxia-specific probes selectively bind to specific biomarkers that are upregulated in hypoxic regions. These probes typically target HIF-1α or its downstream regulators, such as CAIX, glucose transporter-1, vascular endothelial growth factor, and reductive enzymes, including nitroimidazole, nitrobenzyl alcohol, and azobenzene derivatives, which are commonly utilized in both nanoprobes and molecular probes. CAIX is a transmembrane protein overexpressed in hypoxic cells and serves as a prognostic factor in patients with HNC [68]. CAIX is highly expressed in primary and metastatic lesions within several tumor types and is strongly correlated with reduced oxygenation status [69]. Numerous CAIX-targeted antibodies or small-molecule inhibitors have been developed and labeled with fluorophores or radionuclides [22,70]. In a previous study, we synthesized CAIX-800, a dual-motif CAIX ligand conjugated to IRDye 800CW, and demonstrated its targeting efficiency in orthotopic and metastatic NPC models [71]. Future studies must focus on biocompatibility, minimal toxicity, and improved tissue penetration to advance the application of these probes toward clinical trials.

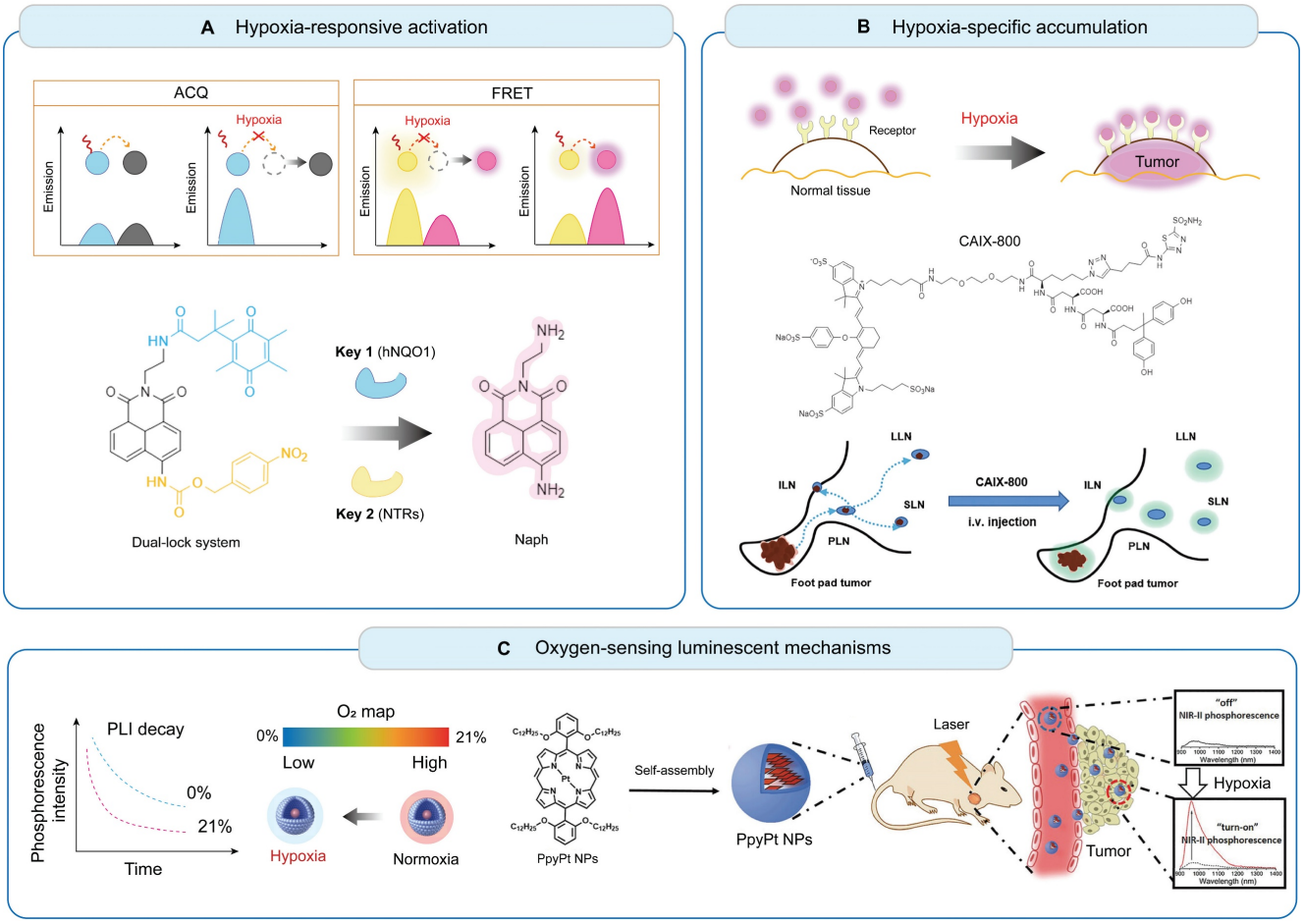

Figure 2. Illustration of the molecular mechanisms and the bioimaging applications of fluorescent hypoxia probes. (A) Hypoxia-responsive activation utilizing FRET and ACQ for enhanced SNR. (B) Hypoxia-specific accumulation targeting hypoxia-induced enzymes or proteins. Adapted with permission from [106], copyright 2022 Springer Nature. (C) Oxygen-sensing luminescent mechanisms based on oxygen-sensitive metal complexes with long-lived emissions. Adapted with permission from [13], copyright 2022 Wiley. FRET: fluorescence resonance energy transfer; ACQ: aggregation-caused quenching; NTRs: nitroreductases; AzoRs: azoreductases; CAIX: carbonic anhydrase IX; SNR: signal-to-noise ratio; PLN, popliteal lymph node; SLN, sciatic lymph node; ILN, inguinal lymph node; LLN, lumbar lymph node.

4.2 Phosphorescence lifetime imaging (PLI)

PLI utilizes oxygen-sensitive phosphorescent molecules to directly quantify O_2 levels using time-resolved cameras. Phosphorescent transition-metal complexes are typical O_2 sensors, including ruthenium, iridium, and metalloporphyrin complexes, which exhibit reversible and linear responses to changes in O_2 concentration [72]. Early-generation probes demonstrate poor water solubility, ultraviolet-visible emission-induced tissue scattering, and limited penetration depth, rendering them unsuitable for *in vivo* studies. Ideally, phosphorescent sensors should exhibit water solubility, low toxicity, high photostability, and NIR emission for deep tissue imaging. Zheng *et al.* developed Ir-PVP, a water-soluble NIR-emitting nanoprobe that enabled the detection of solid tumors and metastatic cancer cells with high sensitivity and SNR [73]. The authors further developed a ratiometric hypoxia imaging nanoprobe by combining semiconducting polymers with phosphorescent phosphors, demonstrating better photostability and lower toxicity than early probes [74]. This probe enabled the quantification of reversible hypoxia (1.56–2.64 mmHg) during radiotherapy. Their findings indicated that the tumor reoxygenation efficiency during the first radiation fraction critically predicted treatment outcomes, highlighting the potential of PLI for optimizing radiation treatment planning. Although PLI offers radiation-free, quantitative, and dynamic hypoxia assessments at a low cost, this technique requires specialized equipment, including lasers and time-resolved cameras, which are complex to set up and operate. A complex imaging system and limited penetration depth may limit its accessibility in clinical settings.

4.3 Photoacoustic imaging (PAI)

PAI employs laser-induced photoacoustic effects and ultrasound detection to visualize biological events at centimeter-level penetration depths. This

technique quantifies oxygen levels and vascular networks by detecting variations in the absorption spectra of endogenous chromophores (such as hemoglobin and melanin) or exogenous contrast agents [75]. Label-free PAI measures oxygenated and deoxygenated hemoglobin concentrations through spectral unmixing and assesses tumor hypoxia based on $_SO_2$ and blood perfusion, which is similar to the principle of BOLD-MRI. This technique offers cost-effective, high-resolution imaging [76-78]. For instance, Ron *et al.* developed a volumetric multispectral optoacoustic tomography system to dynamically capture tumor oxygenation kinetics, distinguishing between normoxic rims, normoxic cores, and hypoxic cores. This novel system sensitively detects cyclic hypoxia, demonstrating potential for therapeutic monitoring [79]. Rich *et al.* used PAI to track tumor oxygenation changes in human papillomavirus (HPV)-positive and -negative xenografts during radiotherapy, indicating the utility of PAI as a radiation response biomarker in patients with HNC [78]. In addition to label-free PAI, advanced techniques utilize exogenous agents to enhance the detection of hypoxia. Tomaszewski *et al.* introduced oxygen-enhanced optoacoustic tomography (OE-OT) and DCE-OT, which revealed strong correlations between *in vivo* imaging parameters (Δ_SO_2 and ΔICG) and *ex vivo* hypoxia quantification [80]. Despite numerous optoacoustic probes that have improved imaging quality, their safety profiles and long-term biocompatibility remain elusive [81,82].

4.4 Cherenkov luminescence imaging (CLI)

CLI is a unique optical imaging technique that captures visible light photons generated when high-energy radiation beams traverse biological tissues. The broadband spectrum of Cherenkov light enables noninvasive quantification of blood oxygenation through the spectral unmixing of oxygenated and deoxygenated hemoglobin absorption profiles. Zhang *et al.* demonstrated a linear correlation between the Cherenkov light intensity and tissue $_SO_2$, facilitating real-time oxygenation monitoring during radiotherapy [83]. Although $_SO_2$ serves as an indirect marker of hypoxia, its relationship with tissue pO_2 remains unclear. Direct pO_2 quantification can be achieved by employing phosphorescent oxygen sensors. Recently, Cherenkov-excited luminescence imaging has been used to quantify tumor hypoxia and its changes during radiation therapy [84-87]. For instance, Pogue *et al.* developed a PtG4 probe that showed preferential accumulation and retention within tumors (>5 days) in breast and HNC xenografts [85] (**Figure 3**). By measuring phosphorescence lifetimes during fractionated radiotherapy (5 Gy per fraction), the authors demonstrated the potential for mapping tumor oxygenation *in vivo* with submillimeter resolution, revealing heterogeneous hypoxic responses across treatment fractions.

Overall, CLI demonstrates considerable potential for assessing therapeutic responses. Combined with oxygen sensors, CLI offers real-time spatial mapping of tissue pO_2 with a submillimeter resolution (~1 mm) for surface imaging. However, two limitations currently limit its clinical application. First, CLI typically provides two-dimensional (2D) images, which hampers accurate signal intensity quantification. Second, it has limited tissue penetration and low sensitivity to deep targets. Future research should prioritize the implementation of 3D tomographic reconstruction techniques and improve oxygen sensors to enhance specificity, sensitivity, biocompatibility, and SNR.

5. Promising Application of Imaging Hypoxia in HNC

With the availability of diverse imaging modalities and innovative probes, hypoxia imaging has demonstrated promising potential for managing patients with HNC. Despite substantial evidence on the feasibility and efficiency of hypoxia-targeted strategies, substantial gaps remain in translating these discoveries into clinically validated techniques. A major obstacle in the clinical trials exploring hypoxia-targeted strategies is the lack of reliable information on tumor hypoxia; thus, there is a pressing need for clinically applicable methodologies that may enable quantification, mapping, and monitoring of hypoxia. We systematically reviewed all relevant clinical trials registered at ClinicalTrials.gov over the past decade (**Table 3**). Most clinical trials have focused on assessing the efficacy of PET-based hypoxia-selective tracers. Given that hypoxia-specific PET imaging is associated with inherent weaknesses, the potential of other methodologies, including MRI and PAI techniques that quantify blood flow or oxygenation-dependent changes, is being explored. While these trials have primarily focused on risk stratification, hypoxia-guided dose escalation, and monitoring of therapeutic response, emerging studies highlight transformative applications in basic science and clinical management of HNC. Next, we elaborate on four promising directions, underscoring the expanding role of hypoxia imaging in precision oncology.

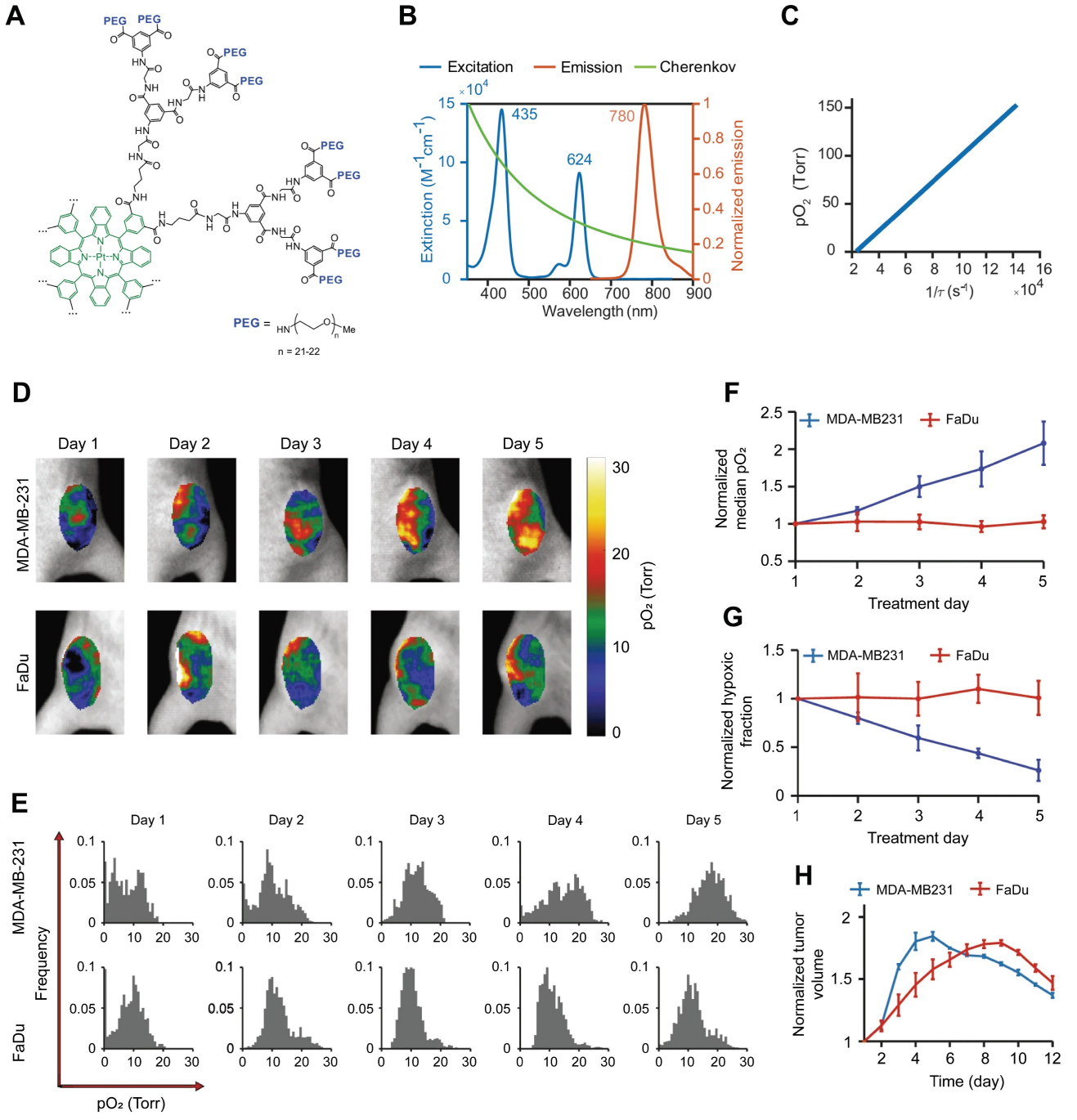

Figure 3. (A) Chemical structure of the phosphorescent oxygen probe Oxyphor PtG4. (B) Excitation and emission spectra of Oxyphor PtG4 and the spectrum of Cherenkov radiation. (C) Oxygen quenching calibration curve of Oxyphor PtG4. (D-E) *In vivo* longitudinal pO_2 imaging of two tumor models over 5 days of fractionated radiotherapy. (F-G) Quantitative analysis of median pO_2 levels and hypoxic fraction changes during treatment. (H) Relative tumor volume changes normalized to baseline prior to radiotherapy. Adapted with permission from [85], an open access article under a CC-BY 4.0 license, copyright 2020 Springer Nature.

Table 3. Clinical trials of hypoxia imaging in HNC.

Study Number	Outcome Measures	Imaging Modality	Tracer	Status	Outcomes	Last Update
NCT03646747	Feasibility of OE-MRI in detecting tumor hypoxia	OE-MRI	Label-free	Unknown Status	NA	2018
NCT04724096	Feasibility of OE-MRI in detecting tumor hypoxia	OE-MRI	Label-free	Completed	OE-MRI was feasible and well-tolerated in detecting hypoxia [113].	2023
NCT01829646	Prognostic value of functional MRI in detecting tumor hypoxia	DCE-MRI and DWI-MRI	Label-free	Recruiting	NA	2023

Study Number	Outcome Measures	Imaging Modality	Tracer	Status	Outcomes	Last Update
NCT03510390	Correlation between hypoxic volume and treatment response	BOLD and DWI	Label-free	Completed	NA	2021
NCT06041555	Feasibility of MRI in detecting tumor hypoxia	multiparametric MR	Label-free	Recruiting	NA	2024
NCT05246475	Voxel-level correlation of hypoxia MRI and PET estimates in detecting hypoxia	multiparametric MR and PET	^{18}F-EF5	Recruiting	NA	2022
NCT06108089	Voxel-level correlation of hypoxia MRI and PET estimates in detecting hypoxia	multiparametric MR and PET	^{18}F-FMISO	Recruiting	NA	2024
NCT05996432	Voxel-level correlation of hypoxia MRI and PET estimates in detecting hypoxia	multiparametric MR and PET	^{18}F-FMISO	Recruiting	NA	2024
NCT04846309	Evaluating the safety and efficiency in hypoxia-guided dose-escalated radiotherapy	multiparametric MR and PET	^{18}F-FMISO	Recruiting	NA	2025
NCT02352792	Prognostic value and relevant toxicity for hypoxia-guided dose-escalated radiotherapy	PET/CT	^{18}F-FMISO	Completed	No relevant toxicities were detected; the dose escalation group experienced a local control benefit [90,111].	2015
NCT01212354	Evaluation of 2-year local control in hypoxia-guided dose-escalated radiotherapy	PET/CT	^{18}F-FMISO	Recruiting	The dose escalation group experienced a 15% local control benefit [92].	2016
NCT01235052	Correlation between hypoxic volume and treatment response	PET/CT	^{18}F-FMISO	Completed	NA	2017
NCT00180180	Correlation of hypoxia between primary tumors and lymph node metastases (LNM)	PET/CT	^{18}F-FMISO	Completed	A significant correlation between FMISO-based hypoxia was observed in the primary tumor and large LNMs [103].	2020
NCT00606294	Evaluating the safety and efficiency in hypoxia-guided treatment optimization	PET/CT	^{18}F-FMISO	Completed	No adverse events were observed; all patients are in the follow-up stage.	2023
NCT00606294	Correlation between hypoxic volume and distant metastasis (DM)	PET/CT	^{18}F-FMISO	Completed	Persistent hypoxia was associated with increased DM risk and worse OS [104].	2023
NCT04995185	Evaluating the feasibility and efficiency of hypoxia-guided dose-escalated radiotherapy	PET/CT	^{18}F-FMISO	Completed	NA	2024
NCT05348486	Evaluating the feasibility and efficiency of hypoxia-guided dose-escalated radiotherapy	PET/CT	^{18}F-FMISO	Recruiting	NA	2025
NCT05544136	Evaluation of overall survival (OS) in hypoxia-guided dose-escalated radiotherapy	PET/CT	^{18}F-FMISO	Recruiting	NA	2025
NCT06087614	Prognostic value and relevant toxicity for hypoxia-guided dose-escalated radiotherapy	PET/CT	^{18}F-FMISO	Recruiting	NA	2025
NCT02207439	Correlation between hypoxic volume and treatment response	PET/CT	^{18}F-FMISO or ^{18}F-EF5	Completed	NA	2023
NCT01017224	Correlation between baseline hypoxia and treatment response	PET/CT	^{18}F-FAZA	Completed	The TMR ≥1.6 at baseline was markedly associated with treatment failure [45].	2012
NCT02976051	Evaluating the efficiency of hypoxia-guided dose-escalated radiotherapy	PET/CT	^{18}F-FAZA	Completed	The dose escalation group achieved a local control benefit of 20% [95].	2020
NCT01075399	Evaluating the repeatability of all parameters in hypoxia PET imaging	PET/CT	^{18}F-HX4	Completed	All parameters were significantly correlated between scans [46].	2013
NCT01347281	Prognostic value for dynamic PET imaging of tumor hypoxia	PET/CT	^{18}F-HX4	Completed	Dynamic changes of hypoxia correlated with prognostic outcome [93].	2017
NCT02976883	Correlation between hypoxic volume and treatment response	PET/CT	^{18}F-HX4	Completed	NA	2019
NCT03003637	Correlation between hypoxic volume and treatment response	PET/CT	^{18}F-HX4	Completed	An on-treatment decrease in hypoxia signature was observed in responders to immunotherapy [97].	2023
NCT06716892	Evaluating the potential of preoperative hypoxia detection in HNC	PAI	Label-free	Recruiting	NA	2024

HNC: head and cancer; PET: positron emission tomography; CT: computed tomography; MR: magnetic resonance; MRI: magnetic resonance imaging; OE-MRI: oxygen-enhanced magnetic resonance imaging; DCE: dynamic contrast-enhanced magnetic resonance imaging; DWI-MRI: diffusion-weighted magnetic resonance imaging; PAI: photoacoustic imaging; NA: not available.

5.1 Guiding radiotherapy: a pending need for convincing evidence

Hypoxic tumor cells exhibit 2–3-fold greater radio-resistance than normoxic cells, contributing to treatment failure and recurrence [12]. Modern radiotherapy techniques, such as intensity-modulated radiation therapy, enable precise dose escalation to subregions within tumors [88]. This has sparked interest in hypoxia-guided dose painting, which allows selective dose escalation within radioresistant regions while sparing adjacent normal tissues. Numerous clinical trials have attempted to validate the feasibility and effectiveness of this strategy [89-95]. For example, a randomized phase II trial (n = 25) assessed the feasibility, toxicity, and efficacy of hypoxia-guided dose escalation [89]. All patients who underwent baseline FMISO PET/CT were randomized to receive standard chemoradiation (70 Gy/35 fractions) or hypoxic volume dose escalation (77 Gy/35 fractions). After a follow-up of 27 months, locoregional control in patients receiving standard radiation was markedly worse than that in those

undergoing dose escalation (44% vs. 100%). Although dose escalation to hypoxic volumes was feasible without increasing toxicity, a subsequent trial (n = 53) failed to detect a significant difference (P = 0.150) in the 5-year locoregional control between the escalated (16/19) and standard (10/17) groups [90] (**Figure 4**). A phase II trial (N = 152) evaluated the feasibility of hypoxia-guided de-escalated chemoradiotherapy using ^{18}F-FMISO PET. Patients with non-hypoxic tumors (n = 128) received 30 Gy of chemotherapy, whereas those with hypoxic tumors (n = 24) received standard chemoradiotherapy at a dose of 70 Gy. The 30-Gy cohort achieved a 2-year locoregional control rate of 94.7% and a 2-year overall survival of 100%, with significantly reduced acute grade 3–4 toxicity (32% vs. 58.3%; P = 0.02) compared with the standard 70-Gy cohort. Based on these findings, hypoxia imaging helped to stratify patients for de-escalated therapy, thereby reducing toxicity while preserving efficacy [91]. The DAHANCA 24 trial prospectively evaluated FAZA PET/CT-defined hypoxia and confirmed its role in the prognostic stratification of patients with non-metastatic HNC (n = 38) undergoing radiotherapy [45]. At a median follow-up of 7.8 years, baseline hypoxia was found to be associated with a 5.8-fold increased risk of locoregional recurrence (44% vs. 9%; hazard ratio [HR] = 5.8), particularly in HPV-negative tumors (57% recurrence). Spatial analysis revealed that recurrence overlapped with baseline hypoxic subvolumes in 2 out of 6 hypoxic cases, supporting the feasibility and efficiency of FAZA PET/CT for guiding treatment intensification. Taken together, while hypoxia-guided dose painting is feasible and well-tolerated, large-scale multicenter trials with extended follow-up periods are necessary to assess its safety and efficacy, optimize patient selection, and standardize hypoxic subvolume delineation protocols.

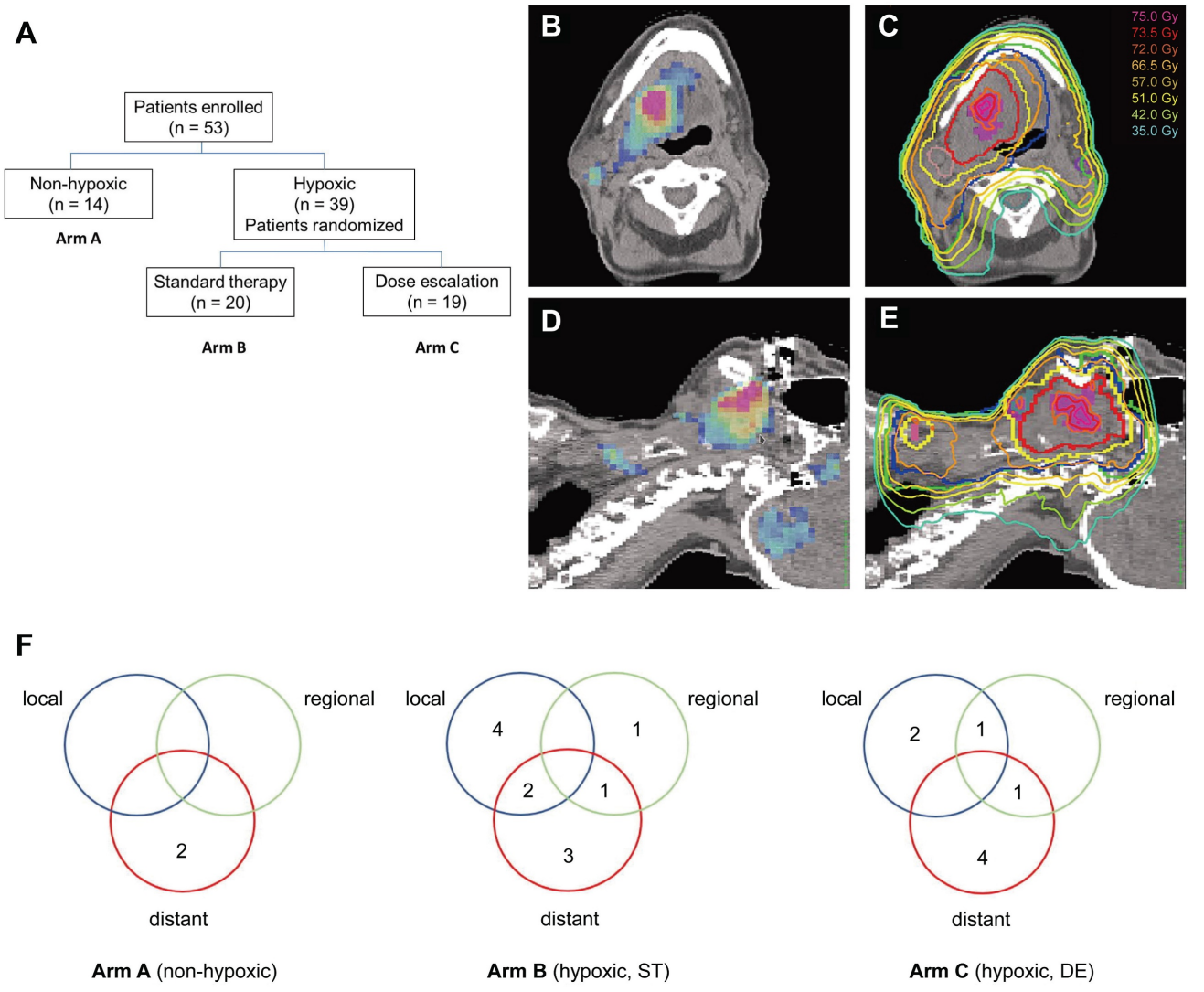

Figure 4. (A) Flowchart of a randomized phase II trial using ^{18}F-FMISO-based PET/CT. (B-E) FMISO PET images (B, D) and corresponding planning CT (C, E) illustrating a dynamic dose painting strategy based on hypoxic subvolumes. (F) Recurrence patterns across treatment arms A, B, and C. Adapted with permission from [90], copyright 2022 Elsevier. PET: positron emission tomography; CT: computed tomography.

5.2 Guiding immunotherapy: an emerging frontier in clinical oncology

Hypoxic tumors promote immunosuppression by recruiting tumor-associated macrophages and inhibiting cytotoxic T-cell activity [96]. Recent findings have identified an association between lymphocyte infiltration and hypoxia, suggesting the potential for hypoxia image-guided immunotherapy [97]. In preclinical models, Reeves *et al.* demonstrated that FMISO-based PET could identify immunosuppressive hypoxic regions, enabling the precise timing of evofosfamide in tumors refractory to programmed cell death protein 1 and cytotoxic T-lymphocyte-associated protein 4 inhibitors [98]. A clinical trial involving 49 patients with HNC demonstrated that an early hypoxic response (assessed via FMISO-based PET) and high tumor-infiltrating lymphocyte levels correlated with improved treatment outcomes [99] (**Figure 5**). The authors successfully established a hypoxia-immunity prognostic scoring system that enables the prediction of treatment responses and outcomes in patients undergoing chemoradiotherapy. Another clinical trial systematically monitored hypoxia evolution using FMISO-based PET imaging at weeks 0, 2, and 5 of the therapy [100]. Patients with persistent hypoxia and high programmed cell death ligand 1 (PD-L1) expression exhibited unfavorable outcomes, whereas those with an early hypoxia response achieved favorable survival regardless of PD-L1 levels. This suggests that combining hypoxia-targeted therapies, immune checkpoint inhibitors, and hypoxia-guided dose escalation could enhance the therapeutic efficacy. Accordingly, hypoxia imaging may stratify patients who would benefit from combined immunotherapy-radiotherapy regimens, although validation in large-scale randomized trials remains critical.

5.3 Tracking metastases: potential for early detection

Current imaging techniques are unable to detect most metastases at an early stage. Tumor hypoxia, a critical driver of metastatic progression, influences multiple steps in the metastatic cascade [101]. Given the genomic consistency between primary tumors and metastases [102], hypoxia may be an attractive target for detecting early metastases. In a cohort of 45 patients with HNC, Bandurska-Luque *et al.* reported a significant but weak correlation between FMISO-based PET hypoxia in primary tumors and metastatic lymph nodes ($r = 0.36$; $P = 0.015$) [103]. In a cohort study of 281 patients with HNC undergoing chemoradiotherapy, persistent hypoxia on FMISO-based PET during treatment was associated with a 3.5-fold increased risk of organ metastasis (HR = 3.51; $P = 0.04$) and worse overall survival (HR = 2.66; $P = 0.02$). None of the patients with baseline hypoxia-negative tumors experienced organ metastasis [104]. Although hypoxia probes have demonstrated satisfactory performance in tumor detection, their application in detecting metastases remains underexplored. Given the established role of CAIX as a promising biomarker of metastatic progression [105], our group developed a CAIX-targeted probe (CAIX-800) and investigated its targeting efficiency in preclinical models, revealing its superior capability to capture clinically undetectable lymph node metastases (< 5 mm) [106]. Accordingly, hypoxia-specific probes, such as CAIX-800, could be promising for detecting micrometastases.

5.4 Screening HAPs: a new frontier in oncology

HAPs selectively release cytotoxic agents in hypoxic tumors with improved therapeutic efficiency [107]. Two HAPs, tirapazamine and evofosfamide, have demonstrated clinical potential despite failing to achieve regulatory approval. The traditional paradigm for assessing the efficacy of HAPs relies on invasive pre- and post-treatment biopsies, underscoring the need for noninvasive hypoxia imaging to monitor the treatment response and evaluate pharmacodynamics [108]. In phase I/II trials involving 44 p16-negative patients with HNC, the combination of tirapazamine plus cisplatin and radiotherapy was assessed using ^{18}F-FMISO-based PET with a 7-year median follow-up, demonstrating a substantial benefit of tirapazamine in locoregional control and progression-free survival in 35 patients with hypoxic tumors [109]. A similar trial using ^{18}F-FAZA-based PET for hypoxia assessment in 41 patients with HPV-negative HNCs confirmed improved locoregional control and failure-free survival with tirapazamine in patients with hypoxic tumors [42]. Furthermore, hypoxia imaging can delineate regions of persistent hypoxia after HAP treatment, indicating drug-resistant niches. Hypoxia imaging may accelerate HAP development and aid in identifying promising candidates for clinical evaluation.

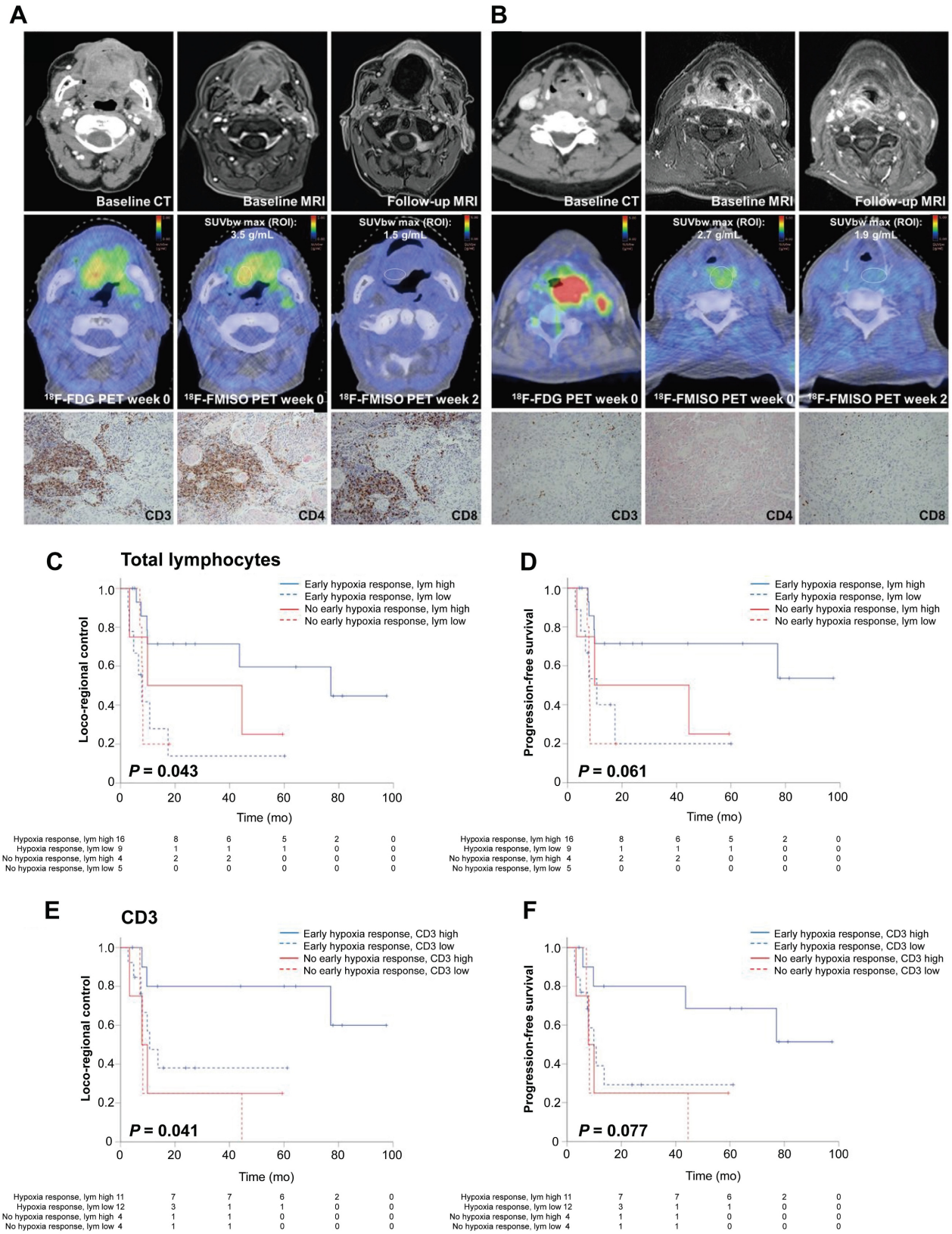

Figure 5. (A-B) Representative patients with HNSCC exhibiting high (A) vs. low (B) intratumoral lymphocyte levels under hypoxic conditions. (C-F) Kaplan-Meier curves showing that early hypoxia resolution and high tumor-infiltrating lymphocyte levels correlate with better outcomes. Adapted with permission from [99], copyright 2021 SNMMI. HNSCC: head and neck squamous cell carcinoma.

6. Challenges and Future Directions

6.1 Current challenges

While PET/CT remains the dominant imaging modality for hypoxia assessment in patients with HNC, most studies primarily utilize the first-generation hypoxia PET tracer (^{18}F-FMISO), which holds clinical promise but exhibits slow tumor diffusion kinetics, suboptimal SNR, and limited spatial resolution [110,111]. Although MRI-based modalities, including OE-MRI, BOLD-MRI, and DCE-MRI, are underexplored in clinical trials, they represent emerging alternatives that leverage endogenous contrast mechanisms without exogenous tracers [112,113]. Notable challenges include technical standardization (e.g., variable oxygen delivery protocols), magnetic susceptibility artifacts at air-tissue interfaces (e.g., oral cavity and sinuses), and the absence of universally accepted MRI-derived hypoxia parameters that correlate with histopathological standards. These drawbacks should be addressed for clinicians to develop MRI as a clinically applicable imaging technique for tumor hypoxia [114]. Despite their high sensitivity and specificity, optical imaging modalities are absent from clinical trials owing to their inherent depth limitations (1–2 cm) [8]. Moreover, the clinical translation of new imaging agents requires a long-term and strict regulatory process, which can explain the gap between basic research and clinical application.

6.2 Multimodal imaging techniques and advanced analytics

With the growing interest in recognizing the complex interactions between hypoxia status and cancer biology and therapy, advances in imaging that reach deeper and broader, ranging from the microscopic to the macroscopic scale, would provide new insights into a comprehensive image of tumor hypoxia and its underlying mechanisms. Multi-imaging modalities integrate the complementary strengths of diverse techniques, address the limitations mentioned above, and offer complementary, accurate, and detailed information [115]. For instance, hybrid PET/MRI combines the high sensitivity of PET with the anatomical and functional resolution of MRI, facilitating the precise delineation of hypoxic regions. The integration of optoacoustic imaging and ultrasound systems enables the unique scalability of spatial resolution and depth penetration across both optical and ultrasonic dimensions, with the potential for the *in vivo* tracking of cyclic hypoxia.

Given the evolving multiparametric data from these integrated systems, analyzing data from different origins with varying temporal and spatial resolutions and formats is a challenging task that requires artificial intelligence (AI)-driven methods [116,117]. A recent study developed a multi-view machine learning framework that synergizes dynamic PET and multiparametric MRI data to characterize intratumoral subregions aligned with tumor histology [116]. AI-based approaches could quantify the phenotypic heterogeneity of hypoxic tumors and predict patient outcomes.

6.3 Advanced study models for future investigations

Current preclinical models do not adequately elucidate the hypoxic heterogeneity in human tumors. Traditional cell line-based animal models fail to reflect the complex biology of parental tumors [118]. Although patient-derived xenografts, generated by transplanting patient-derived tumor samples into mice, are closer to ideal models, they are expensive and time-consuming. Tumor organoids or 3D cell culture systems derived from patient tumor tissues offer physiologically relevant platforms for examining tumor hypoxia [119,120]. Culturing under controlled oxygen gradients and stromal interactions enables high-throughput screening of hypoxia-targeted agents (e.g., HAPs and imaging probes) and real-time tracking of therapeutic responses [121]. Such a robust and versatile platform can enable personalized and precise imaging of tumor hypoxia.

7. Conclusions

Hypoxia imaging has emerged as a critical tool for managing patients with HNC, and recent advancements have considerably improved the detection and longitudinal monitoring of tumor hypoxia. Each imaging technique offers unique advantages and insights, and their integration provides a comprehensive view of tumor oxygenation and related biological processes. In addition to diagnosis, hypoxia imaging plays a pivotal role in guiding personalized treatment strategies such as hypoxia-guided radiotherapy or immunotherapy, optimization of HAP synthesis, and hypoxia-targeted delivery of immune checkpoint inhibitors.

Despite notable advances, existing hypoxia-targeted probes have several limitations, including suboptimal specificity, limited tissue penetration (especially in optical probes), potential off-target reactivity, and complex synthesis routes. Imaging devices also encounter challenges, such as low spatial resolution (PET/CT), susceptibility artifacts (MRI), and shallow imaging depth (optical techniques), which collectively impede their clinical utility. Furthermore, regulatory hurdles and the lack

of standardized validation models contribute to the translational gap.

Future directions include improving probe safety profiles, simplifying synthesis routes, exploring NIR-II platforms for improved depth, and integrating multimodal imaging systems to enhance translational potential. Simultaneously, 3D preclinical models, including patient-derived tumor organoids, large-scale multicenter trials, and AI-driven analytics, will be valuable in identifying robust hypoxia imaging biomarkers. Collectively, these efforts will help overcome current barriers and maximize the potential of hypoxia imaging in precision oncology, ultimately improving therapeutic outcomes in patients with HNC.

Abbreviations

HNC: head and neck cancer; PET: positron emission tomography; MRI: magnetic resonance imaging; O_2: oxygen; CT: computed tomography; ^{18}F-FAZA: [^{18}F] fluoroazomycin arabinoside; ^{18}F-HX4: [^{18}F] flortanidazole; ^{18}F-FMISO: [^{18}F] fluoromisonidazole; OMI: optical molecular imaging; HAPs: hypoxia-activated prodrugs; pO_2: partial oxygen pressure; $_SO_2$: oxygen saturation; CAIX: carbonic anhydrase IX; NTRs: nitroreductases; AzoRs: azoreductases; H_2O_2: hydrogen peroxide; H_2S: hydrogen sulfide; HIF-1α: hypoxia-inducible factor-1α; SNR: signal-to-noise ratio; TBR: tumor-background ratio; BOLD-MRI: blood oxygen level-dependent MRI; OE-MRI: oxygen-enhanced MRI; DCE-MRI: dynamic contrast-enhanced MRI; OMI: optical molecular imaging; ACQ: aggregation-caused quenching; FRET: fluorescence resonance energy transfer; PLI: phosphorescence lifetime imaging; PAI: photoacoustic imaging; OE-OT: oxygen-enhanced optoacoustic tomography; DCE-OT: dynamic contrast-enhanced optoacoustic tomography; CLI: Cherenkov luminescence imaging; PD-L1: programmed cell death ligand 1; AI: artificial intelligence.

Acknowledgments

Funding

We would like to thank Editage (www.editage .cn) for English language editing and Figdraw for diagrams modification (https://www.figdraw .com/). We acknowledge financial support from the National Key Research and Development Program of China (2023YFF1204600), the National Natural Science Foundation of China (82227802, 82272029, 82302336), the Beijing Science Fund for Distinguished Young Scholars (JQ22013), the Science and Technology Projects in Guangzhou (2023A03J1036), the Natural Science Foundation of Guangdong Province of China (2025A1515012336), and the Postdoctoral Science Foundation of China (2024M751132).

Author contributions

Shuixing Zhang, Kun Wang and Jie Tian conceived and designed this study. Wenhui Huang and Nemin Li wrote the initial draft of the manuscript. Xinyang Song and Yuze Zhang performed the literature review and analysis. Wenhui Huang, Nemin Li, and Sheng Zhu designed tables and figures. Bin Zhang and Hao Yan provided feedback on the scientific accuracy and clarity of the manuscript. Shuixing Zhang completed the final revision and ensured the quality and coherence of the manuscript. All the authors have read and approved the final version of the manuscript.

Competing Interests

The authors have declared that no competing interest exists.

References

1. Johnson DE, Burtness B, Leemans CR, Lui VWY, Bauman JE, Grandis JR. Head and neck squamous cell carcinoma. Nat Rev Dis Primers. 2020; 6: 92.
2. Colevas AD, Cmelak AJ, Pfister DG, Spencer S, Adkins D, Birkeland AC, et al. NCCN guidelines® insights: head and neck cancers, version 2.2025. J Natl Compr Canc Netw. 2025; 23: 211.
3. Chen Z, Han F, Du Y, Shi H, Zhou W. Hypoxic microenvironment in cancer: molecular mechanisms and therapeutic interventions. Signal Transduct Target Ther. 2023; 8: 70.
4. Horsman MR, Mortensen LS, Petersen JB, Busk M, Overgaard J. Imaging hypoxia to improve radiotherapy outcome. Nat Rev Clin Oncol. 2012; 9: 674-87.
5. Bhandari V, Hoey C, Liu LY, Lalonde E, Ray J, Livingstone J, et al. Molecular landmarks of tumor hypoxia across cancer types. Nat Genet. 2019; 51: 308-18.
6. Bhandari V, Li CH, Bristow RG, Boutros PC; PCAWG Consortium. Divergent mutational processes distinguish hypoxic and normoxic tumours. Nat Commun. 2020; 11: 737.
7. Perez RC, Kim D, Maxwell AWP, Camacho JC. Functional imaging of hypoxia: PET and MRI. Cancers. 2023; 15: 3336.
8. Cheng MHY, Mo Y, Zheng G. Nano versus molecular: optical imaging approaches to detect and monitor tumor hypoxia. Adv Healthc Mater. 2020; 10: e2001549.
9. Liu JN, Bu W, Shi J. Chemical design and synthesis of functionalized probes for imaging and treating tumor hypoxia. Chem Rev. 2017; 117: 6160-224.
10. Baran N, Konopleva M. Molecular pathways: hypoxia-activated prodrugs in cancer therapy. Clin Cancer Res. 2017; 23: 2382-90.
11. O'Connor LJ, Cazares-Körner C, Saha J, Evans CN, Stratford MR, Hammond EM, et al. Design, synthesis and evaluation of molecularly targeted hypoxia-activated prodrugs. Nat Protoc. 2016; 11: 781-94.
12. Singleton DC, Macann A, Wilson WR. Therapeutic targeting of the hypoxic tumour microenvironment. Nat Rev Clin Oncol. 2021; 18: 751-72.
13. Zhang WS, Chen SY, Sun PF, Ye S, Fan QL, Song J, et al. NIR-II J-aggregated Pt(II)-porphyrin-based phosphorescent probe for tumor-hypoxia imaging. Adv Healthc Mater. 2022; 11: e2200467.
14. Liu CY, Sadhu AS, Karmakar R, Chu CS, Lin YN, Chang SH, et al. Strongly improving the sensitivity of phosphorescence-based optical oxygen sensors by exploiting nano-porous substrates. Biosensors (Basel). 2022; 12: 774.
15. Wu CH, Kisel KS, Thangavel MK, Chen YT, Chang KH, Tsai MR, et al. Functionalizing collagen with vessel-penetrating two-photon phosphorescence probes: A new in vivo strategy to map oxygen concentration in tumor microenvironment and tissue ischemia. Adv Sci (Weinh). 2021; 8: e2102788.
16. Wang Z, Zhang S, Kong Z, Li S, Sun J, Zheng Y, et al. Self-adaptive nanoassembly enabling turn-on hypoxia illumination and periphery/center closed-loop tumor eradication. Cell Rep Med. 2023; 4: 101014.
17. Guisán-Ceinos S, R Rivero A, Romeo-Gella F, Simón-Fuente S, Gómez-Pastor S, Calvo N, et al. Turn-on fluorescent biosensors for imaging hypoxia-like conditions in living cells. J Am Chem Soc. 2022; 144: 8185-93.

18. Zhang Y, Zhao W, Chen Y, Yuan H, Fang H, Yao S, et al. Rational construction of a reversible arylazo-based NIR probe for cycling hypoxia imaging in vivo. Nat Commun. 2021; 12: 2772.
19. Yu C, Wang S, Xu C, Ding Y, Zhang G, Yang N, et al. Two-photon small-molecule fluorogenic probes for visualizing endogenous nitroreductase activities from tumor tissues of a cancer patient. Adv Healthc Mater. 2022; 11: e2200400.
20. Sun X, Xu L, Xu H-D, Xie L, Wang R, Yang Z, et al. Intracellular nitroreductase-triggered "on" and "enhanced" photoacoustic signals for sensitive imaging of tumor hypoxia. Adv Healthc Mater. 2024; 13: e2303472.
21. Takacova M, Kajanova I, Kolarcikova M, Lapinova J, Zatovicova M, Pastorekova S. Understanding metabolic alterations and heterogeneity in cancer progression through validated immunodetection of key molecular components: a case of carbonic anhydrase IX. Cancer Metastasis Rev. 2021; 40: 1035-53.
22. Chen KT, Seimbille Y. New developments in carbonic anhydrase IX-targeted fluorescence and nuclear imaging agents. Int J Mol Sci. 2022; 23: 6125.
23. Goel S, Shi S. Promise of hypoxia-targeted tracers in metastatic lymph node imaging. Eur J Nucl Med Mol Imaging. 2022; 49: 4293-7.
24. Zhou S, Jiang L, Li C, Mao H, Jiang C, Wang Z, et al. Acid and hypoxia tandem-activatable deep near-infrared nanoprobe for two-step signal amplification and early detection of cancer. Adv Mater. 2023; 35: e2212231.
25. Chang Z, Niu T, Shao Q, Yue J, Zhang H, Tong L, et al. Pt-Se-bonded nanoprobe for high-fidelity detection of non-small cell lung cancer and enhancement of NIR II photothermal therapy. Anal Chem. 2023; 95: 18426-35.
26. Chen Z, Su L, Wu Y, Liu J, Wu R, Li Q, et al. Design and synthesis of a small molecular NIR-II chemiluminescence probe for in vivo-activated H_2S imaging. Proc Natl Acad Sci U S A. 2023; 120: e2205186120.
27. Zhao XB, Kang JY, Shi YP. Noncovalent dual-locked near-infrared fluorescent probe for precise imaging of tumor via hypoxia/glutathione activation. Anal Chem. 2022; 94: 6574-81.
28. Peng H, Wang T, Li G, Huang J, Yuan Q. Dual-locked near-infrared fluorescent probes for precise detection of melanoma via hydrogen peroxide-tyrosinase cascade activation. Anal Chem. 2022; 94: 1070-5.
29. Hong SJ, Jeon E, Kim MJ, Lee MH. Dual-lock system for high sensitivity and selectivity in redox enzyme activation and imaging. Anal Chem. 2025; 97: 1143-50.
30. Yoon SA, Hong SJ, Han J, Lee MH. Sensitive cancer hypoxia detection via a dual-locking fluorescence response system using two hypoxia indicators. Anal Chem. 2024; 96: 15372-9.
31. Wen Y, Zhang S, Yuan W, Feng W, Li F. Afterglow/fluorescence dual-emissive ratiometric oxygen probe for tumor hypoxia imaging. Anal Chem. 2023; 95: 2478-86.
32. Ge L, Tang Y, Wang C, Chen J, Mao H, Jiang X. A light-activatable theranostic combination for ratiometric hypoxia imaging and oxygen-deprived drug activity enhancement. Nat Commun. 2024; 15: 153.
33. Marcus C, Subramaniam RM. Role of Non-FDG-PET/CT in head and neck cancer. Semin Nucl Med. 2021; 51: 68-78.
34. Nario AP, Woodfield J, dos Santos SN, Bergman C, Wuest M, Araújo YB, et al. Synthesis of a 2-nitroimidazole derivative N-(4-[^{18}F]fluorobenzyl)-2-(2-nitro-1H-imidazol-1-yl)-acetamide ([^{18}F]FBNA) as PET radiotracer for imaging tumor hypoxia. EJNMMI Radiopharm Chem. 2022; 7: 13.
35. Zschaeck S, Löck S, Hofheinz F, Zips D, Saksø Mortensen L, Zöphel K, et al. Individual patient data meta-analysis of FMISO and FAZA hypoxia PET scans from head and neck cancer patients undergoing definitive radio-chemotherapy. Radiother Oncol. 2020; 149: 189-96.
36. Nicolay NH, Wiedenmann N, Mix M, Weber WA, Werner M, Grosu AL, et al. Correlative analyses between tissue-based hypoxia biomarkers and hypoxia PET imaging in head and neck cancer patients during radiochemotherapy-results from a prospective trial. Eur J Nucl Med Mol Imaging. 2020; 47: 1046-55.
37. Hildingsson S, Gebre-Medhin M, Zschaeck S, Adrian G. Hypoxia in relationship to tumor volume using hypoxia PET-imaging in head & neck cancer - A scoping review. Clin Transl Radiat Oncol. 2022; 36: 40-6.
38. Zschaeck S, Haase R, Abolmaali N, Perrin R, Stützer K, Appold S, et al. Spatial distribution of FMISO in head and neck squamous cell carcinomas during radio-chemotherapy and its correlation to pattern of failure. Acta Oncol. 2015; 54: 1355-63.
39. Sato J, Kitagawa Y, Watanabe S, Asaka T, Ohga N, Hirata K, et al. Hypoxic volume evaluated by ^{18}F-fluoromisonidazole positron emission tomography (FMISO-PET) may be a prognostic factor in patients with oral squamous cell carcinoma: preliminary analyses. Int J Oral Maxillofac Surg. 2018; 47: 553-60.
40. Löck S, Linge A, Seidlitz A, Bandurska-Luque A, Nowak A, Gudziol V, et al. Repeat FMISO-PET imaging weakly correlates with hypoxia-associated gene expressions for locally advanced HNSCC treated by primary radiochemotherapy. Radiother Oncol. 2019; 135: 43-50.
41. Silvoniemi A, Suilamo S, Laitinen T, Forsback S, Löyttyniemi E, Vaittinen S, et al. Repeatability of tumour hypoxia imaging using [^{18}F]EF5 PET/CT in head and neck cancer. Eur J Nucl Med Mol Imaging. 2018; 45: 161-9.
42. Graves EE, Hicks RJ, Binns D, Bressel M, Le Q-T, Peters L, et al. Quantitative and qualitative analysis of [(18)F]FDG and [(18)F]FAZA positron emission tomography of head and neck cancers and associations with HPV status and treatment outcome. Eur J Nucl Med Mol Imaging. 2016; 43: 617-25.
43. Sanduleanu S, Wiel AMAV, Lieverse RIY, Marcus D, Ibrahim A, Primakov S, et al. Hypoxia PET imaging with [^{18}F]-HX4-A promising next-generation tracer. Cancers (Basel). 2020; 12: 1322.
44. Saga T, Inubushi M, Koizumi M, Yoshikawa K, Zhang M-R, Obata T, et al. Prognostic value of PET/CT with (18)F-fluoroazomycin arabinoside for patients with head and neck squamous cell carcinomas receiving chemoradiotherapy. Ann Nucl Med. 2016; 30: 217-24.
45. Saksø M, Mortensen LS, Primdahl H, Johansen J, Kallehauge J, Hansen CR, et al. Influence of FAZA PET hypoxia and HPV-status for the outcome of head and neck squamous cell carcinoma (HNSCC) treated with radiotherapy: Long-term results from the DAHANCA 24 trial (NCT01017224). Radiother Oncol. 2020; 151: 126-33.
46. Zegers CM, van Elmpt W, Szardenings K, Kolb H, Waxman A, Subramaniam RM, et al. Repeatability of hypoxia PET imaging using [^{18}F]HX4 in lung and head and neck cancer patients: a prospective multicenter trial. Eur J Nucl Med Mol Imaging. 2015; 42: 1840-9.
47. Carlin S, Zhang H, Reese M, Ramos NN, Chen Q, Ricketts SA. A comparison of the imaging characteristics and microregional distribution of 4 hypoxia PET tracers. J Nucl Med. 2014; 55: 515-21.
48. Busk M, Overgaard J, Horsman MR. Imaging of tumor hypoxia for radiotherapy: current status and future directions. Semin Nucl Med. 2020; 50: 562-83.
49. Panek R, Welsh L, Baker LCJ, Schmidt MA, Wong KH, Riddell AM, et al. Noninvasive imaging of cycling hypoxia in head and neck cancer using intrinsic susceptibility MRI. Clin Cancer Res. 2017; 23: 4233-41.
50. Panek R, Welsh L, Dunlop A, Wong KH, Riddell AM, Koh D-M, et al. Repeatability and sensitivity of T2* measurements in patients with head and neck squamous cell carcinoma at 3T. J Magn Reson Imaging. 2016; 44: 72-80.
51. Hallac RR, Zhou H, Pidikiti R, Song K, Stojadinovic S, Zhao D, et al. Correlations of noninvasive BOLD and TOLD MRI with pO_2 and relevance to tumor radiation response. Magn Reson Med. 2014; 71: 1863-73.
52. Wiedenmann N, Bunea H, Rischke HC, Bunea A, Majerus L, Bielak L, et al. Effect of radiochemotherapy on T2* MRI in HNSCC and its relation to FMISO PET derived hypoxia and FDG PET. Radiat Oncol. 2018; 13: 159.
53. Virani N, Kwon J, Zhou H, Mason R, Berbeco R, Protti A. In vivo hypoxia characterization using blood oxygen level dependent magnetic resonance imaging in a preclinical glioblastoma mouse model. Magn Reson Imaging. 2021; 76: 52-60.
54. O'Connor JPB, Robinson SP, Waterton JC. Imaging tumour hypoxia with oxygen-enhanced MRI and BOLD MRI. Br J Radiol. 2019; 92: 20180642.
55. O'Connor JPB, Boult JKR, Jamin Y, Babur M, Finegan KG, Williams KJ, et al. Oxygen-enhanced MRI accurately identifies, quantifies, and maps tumor hypoxia in preclinical cancer models. Cancer Res. 2016; 76: 787-95.
56. Salem A, Little RA, Latif A, Featherstone AK, Babur M, Peset I, et al. Oxygen-enhanced MRI is feasible, repeatable, and detects radiotherapy-induced change in hypoxia in xenograft models and in patients with non-small cell lung cancer. Clin Cancer Res. 2019; 25: 3818-29.
57. Dubec MJ, Buckley DL, Berks M, Clough A, Gaffney J, Datta A, et al. First-in-human technique translation of oxygen-enhanced MRI to an MR Linac system in patients with head and neck cancer. Radiother Oncol. 2023; 183: 109592.
58. McCabe A, Martin S, Shah J, Morgan PS, Panek R. T_1 based oxygen-enhanced MRI in tumours; a scoping review of current research. Br J Radiol. 2023; 96: 20220624.
59. Little RA, Jamin Y, Boult JKR, Naish JH, Watson Y, Cheung S, et al. Mapping hypoxia in renal carcinoma with oxygen-enhanced MRI: comparison with intrinsic susceptibility MRI and pathology. Radiology. 2018; 28: 739-47.
60. Gaddikeri S, Gaddikeri RS, Tailor T, Anzai Y. Dynamic contrast-enhanced MR imaging in head and neck cancer: techniques and clinical applications. AJNR Am J Neuroradiol. 2016; 37: 588-95.
61. Gaustad J-V, Hauge A, Wegner CS, Simonsen TG, Lund KV, Hansem LMK, et al. DCE-MRI of tumor hypoxia and hypoxia-associated aggressiveness. Cancers. 2020; 12: 1979.
62. Bernstein JM, Homer JJ, West CM. Dynamic contrast-enhanced magnetic resonance imaging biomarkers in head and neck cancer: potential to guide treatment? A systematic review. Oral Oncol. 2014; 50: 963-70.
63. Xue F, Chen J, Chen H. Design strategy of optical probes for tumor hypoxia imaging. Sci China Life Sci. 2020; 63: 1786-97.
64. Luby BM, Charron DM, MacLaughlin CM, Zheng G. Activatable fluorescence: From small molecule to nanoparticle. Adv Drug Deliv Rev. 2017; 113: 97-121.
65. Cheng HB, Zhang S, Qi J, Liang XJ, Yoon J. Advances in Application of Azobenzene as a Trigger in Biomedicine: Molecular Design and Spontaneous Assembly. Adv Mater. 2021; 33: e2007290.
66. Zheng ZL, Chen XJ, Dai R, Wu ST, Kang WW, Qin YF, et al. Cyclic enhancement of hypoxic microenvironment via an intelligent nanoamplifier for activated NIR-II fluorescence/photoacoustic imaging-guided precise synergistic therapy. Mater Today Bio. 2022; 17: 100478.
67. Hu C, Liu H, Zhang Z, Li L, Mao G-J, Cheng W, et al. A self-calibrating fluorescent-photoacoustic integrated probe enables fast visualizing pancreatic cancer and imaging-guided tumor surgery. Small. 2024; 21: e2408527.
68. Huizing FJ, Hoeben BAW, Franssen GM, Boerman OC, Heskamp S, Bussink J. Quantitative imaging of the hypoxia-related marker CAIX in head and neck squamous cell carcinoma xenograft models. Mol Pharm. 2018; 16: 701-8.
69. Huizing FJ, Hoeben BAW, Lok J, Boerman OC, Heskamp S, Bussink J. Imaging carbonic anhydrase IX as a method for monitoring hypoxia-related

radioresistance in preclinical head and neck cancer models. Phys Imaging Radiat Oncol. 2021; 19: 145-50.
70. Kulterer OC, Pfaff S, Wadsak W, Garstka N, Remzi M, Vraka C, et al. A microdosing study with ^{99m}Tc-PHC-102 for the SPECT/CT imaging of primary and metastatic lesions in renal cell carcinoma patients. J Nucl Med. 2021; 62: 360-5.
71. Huang W, Wang K, An Y, Meng H, Gao Y, Xiong Z, et al. In vivo three-dimensional evaluation of tumour hypoxia in nasopharyngeal carcinomas using FMT-CT and MSOT. Eur J Nucl Med Mol Imaging. 2019; 47: 1027-38.
72. Xiao P, Liu CY, Ma TC, Lu XH, Jing LH, Hou Y, et al. A cyclodextrin-hosted Ir(III) complex for ratiometric mapping of tumor hypoxia in vivo. Adv Sci. 2021; 8: 2004044.
73. Zheng X, Wang X, Mao H, Wu W, Liu B, Jiang X. Hypoxia-specific ultrasensitive detection of tumours and cancer cells in vivo. Nat Commun. 2015; 6: 5834.
74. Zheng X, Cui L, Chen M, Soto LA, Graves EE, Rao J. A near-infrared phosphorescent nanoprobe enables quantitative, longitudinal imaging of tumor hypoxia dynamics during radiotherapy. Cancer Res. 2019; 79: 4787-97.
75. Attia ABE, Balasundaram G, Moothanchery M, Dinish US, Bi R, Ntziachristos V, et al. A review of clinical photoacoustic imaging: current and future trends. Photoacoustics. 2019; 16: 100144.
76. Klibanov AL, Hu S. Monitoring oxygenation levels deep in the tumor core: noninvasive imaging of hypoxia, now in real-time 3D. Cancer Res. 2019; 79: 4577-9.
77. Tomaszewski MR, Gehrung M, Joseph J, Quiros-Gonzalez I, Disselhorst JA, Bohndiek SE. Oxygen-enhanced and dynamic contrast-enhanced optoacoustic tomography provide surrogate biomarkers of tumor vascular function, hypoxia, and necrosis. Cancer Res. 2018; 78: 5980-91.
78. Rich LJ, Miller A, Singh AK, Seshadri M. Photoacoustic imaging as an early biomarker of radio therapeutic efficacy in head and neck cancer. Theranostics. 2018; 8: 2064-78.
79. Ron A, Deán-Ben XL, Gottschalk S, Razansky D. Volumetric optoacoustic imaging unveils high-resolution patterns of acute and cyclic hypoxia in a murine model of breast cancer. Cancer Res. 2019; 79: 4767-75.
80. Tomaszewski MR, Gonzalez IQ, O'Connor JPB, Abeyakoon O, Parker GJM, Williams KJ, et al. Oxygen enhanced optoacoustic tomography (OE-OT) reveals vascular dynamics in murine models of prostate cancer. Theranostics. 2017; 7: 2900-13.
81. Nasri D, Manwar R, Kaushik A, Er EE, Avanaki K. Photoacoustic imaging for investigating tumor hypoxia: a strategic assessment. Theranostics. 2023; 13: 3346-67.
82. Weber, J, Beard, PC, Bohndiek, SE. Contrast agents for molecular photoacoustic imaging. Nat Methods. 2016; 13: 639-50.
83. Zhang X, Lam SK, Palmer G, Das S, Oldham M, Dewhirst M. Noninvasive measurement of tissue blood oxygenation with Cerenkov imaging during therapeutic radiation delivery. Opt Lett. 2017; 42: 3101-4.
84. Pogue BW, Cao X, Swartz HM, Vinogradov S. Review of tissue oxygenation sensing during radiotherapy based upon Cherenkov-excited luminescence imaging. Appl Magn Reson. 2021; 52: 1521-36.
85. Cao X, Rao Allu S, Jiang S, Jia M, Gunn JR, Yao C, et al. Tissue pO_2 distributions in xenograft tumors dynamically imaged by Cherenkov-excited phosphorescence during fractionated radiation therapy. Nat Commun. 2020; 11: 573.
86. Cao X, Allu SR, Jiang S, Gunn Bs JR, Yao C, Xin J, et al. High-resolution pO_2 imaging improves quantification of the hypoxic fraction in tumors during radiation therapy. Int J Radiat Oncol Biol Phys. 2021; 109: 603-13.
87. Cao X, Gunn JR, Allu SR, Bruza P, Jiang S, Vinogradov SA, et al. Implantable sensor for local Cherenkov-excited luminescence imaging of tumor pO_2 during radiotherapy. J Biomed Opt. 2020; 25: 112704.
88. Riaz N, Sherman E, Pei X, Schöder H, Grkovski M, Paudyal R, et al. Precision radiotherapy: reduction in radiation for oropharyngeal cancer in the 30 ROC trial. J Natl Cancer Inst. 2021; 113: 742-51.
89. Welz S, Mönnich D, Pfannenberg C, Nikolaou K, Reimold M, La Fougère C, et al. Prognostic value of dynamic hypoxia PET in head and neck cancer: Results from a planned interim analysis of a randomized phase II hypoxia-image guided dose escalation trial. Radiother Oncol. 2017; 124: 526-32.
90. Welz S, Paulsen F, Pfannenberg C, Reimold M, Reischl G, Nikolaou K, et al. Dose escalation to hypoxic subvolumes in head and neck cancer: A randomized phase II study using dynamic [^{18}F]FMISO PET/CT. Radiother Oncol. 2022; 171: 30-6.
91. Lee NY, Sherman EJ, Schöder H, Wray R, Boyle JO, Singh B, et al. Hypoxia-directed treatment of human papillomavirus-related oropharyngeal carcinoma. J Clin Oncol. 2024; 42: 940-50.
92. Pigorsch SU, Wilkens JJ, Kampfer S, Kehl V, Hapfelmeier A, Schläger C, et al. Do selective radiation dose escalation and tumour hypoxia status impact the loco-regional tumour control after radio-chemotherapy of head & neck tumours? The ESCALOX protocol. Radiat Oncol. 2017; 12: 45.
93. Sanduleanu S, Hamming-Vrieze O, Wesseling FWR, Even AJG, Hoebers FJ, Hoeben A, et al. [^{18}F]-HX4 PET/CT hypoxia in patients with squamous cell carcinoma of the head and neck treated with chemoradiotherapy: Prognostic results from two prospective trials. Clin Transl Radiat Oncol. 2020; 23: 9-15.
94. Lee N, Schoder H, Beattie B, Lanning R, Riaz N, McBride S, et al. Strategy of using intratreatment hypoxia imaging to selectively and safely guide radiation dose de-escalation concurrent with chemotherapy for locoregionally advanced human papillomavirus-related oropharyngeal carcinoma. Int J Radiat Oncol Biol Phys. 2016; 96: 9-17.
95. Saksø M, Primdahl H, Johansen J, Nowicka-Matus K, Overgaard J; DAHANCA. DAHANCA 33: functional image-guided dose-escalated radiotherapy to patients with hypoxic squamous cell carcinoma of the head and neck (NCT02976051). Acta Oncol. 2020; 59: 208-11.
96. Sattiraju A, Kang S, Giotti B, Chen Z, Marallano VJ, Brusco C, et al. Hypoxic niches attract and sequester tumor-associated macrophages and cytotoxic T cells and reprogram them for immunosuppression. Immunity. 2023; 56: 1825-43.e6.
97. Vos JL, Elbers JBW, Krijgsman O, Traets JJH, Qiao X, van der Leun AM, et al. Neoadjuvant immunotherapy with nivolumab and ipilimumab induces major pathological responses in patients with head and neck squamous cell carcinoma. Nat Commun. 2021; 12: 7348.
98. Reeves KM, Song PN, Angermeier A, Manna DD, Li Y, Wang J, et al. ^{18}F-FMISO PET imaging identifies hypoxia and immunosuppressive tumor microenvironments and guides targeted evofosfamide therapy in tumors refractory to PD-1 and CTLA-4 inhibition. Clin Cancer Res. 2022; 28: 327-37.
99. Nicolay NH, Rühle A, Wiedenmann N, Niedermann G, Mix M, Weber WA, et al. Lymphocyte infiltration determines the hypoxia-dependent response to definitive chemoradiation in head-and-neck cancer: results from a prospective imaging trial. J Nucl Med. 2021; 62: 471-8.
100. Rühle A, Grosu A-L, Wiedenmann N, Mix M, Stoian R, Niedermann G, et al. Hypoxia dynamics on FMISO-PET in combination with PD-1/PD-L1 expression has an impact on the clinical outcome of patients with head-and-neck squamous cell carcinoma undergoing chemoradiation. Theranostics. 2020; 10: 9395-406.
101. Rankin EB, Giaccia AJ. Hypoxic control of metastasis. Science. 2016; 352: 175-80.
102. Priestley P, Baber J, Lolkema MP, Steeghs N, de Bruijn E, Shale C, et al. Pan-cancer whole-genome analyses of metastatic solid tumours. Nature. 2019; 575: 210-6.
103. Bandurska-Luque A, Löck S, Haase R, Richter C, Zöphel K, Perrin R, et al. Correlation between FMISO-PET based hypoxia in the primary tumour and in lymph node metastases in locally advanced HNSCC patients. Clin. Transl Radiat Oncol. 2019; 15: 108-12.
104. Gui C, Wray R, Schöder H, Deasy JO, Grkovski M, Humm JL, et al. Tumor hypoxia on ^{18}F-fluoromisonidazole positron emission tomography and distant metastasis from head and neck squamous cell carcinoma. JAMA Netw Open. 2024; 7: e2436407.
105. Pastorekova S, Gillies RJ. The role of carbonic anhydrase IX in cancer development: links to hypoxia, acidosis, and beyond. Cancer Metastasis Rev. 2019; 38: 65-77.
106. Huang W, Wang K, Huang W, He Z, Zhang J, Zhang B, et al. Carbonic anhydrase IX stratifies patient prognosis and identifies nodal status in animal models of nasopharyngeal carcinoma using a targeted imaging strategy. Eur J Nucl Med Mol Imaging. 2022; 49: 4427-39.
107. van der Wiel AMA, Jackson-Patel V, Niemans R, Yaromina A, Liu E, Marcus D, et al. Selectively targeting tumor hypoxia with the hypoxia-activated prodrug CP-506. Mol Cancer Ther. 2021; 20: 2372-83.
108. Hegde A, Jayaprakash P, Couillault CA, Piha-Paul S, Karp D, Rodon J, et al. A phase I dose-escalation study to evaluate the safety and tolerability of evofosfamide in combination with ipilimumab in advanced solid malignancies. Clin Cancer Res 2021; 27: 3050-60.
109. Trinkaus ME, Hicks RJ, Young RJ, Peters LJ, Solomon B, Bressel M, et al. Correlation of p16 status, hypoxic imaging using [^{18}F]-misonidazole positron emission tomography and outcome in patients with loco-regionally advanced head and neck cancer. J Med Imaging Radiat Oncol. 2014; 58: 89-97.
110. Wray R, Mauguen A, Michaud L, Leithner D, Yeh R, Riaz N, et al. Development of ^{18}F-fluoromisonidazole hypoxia PET/CT diagnostic interpretation criteria and validation of interreader reliability, reproducibility, and performance. J Nucl Med. 2024; 65: 1526-32.
111. Boeke S, Thorwarth D, Mönnich D, Pfannenberg C, Reischl G, La Fougère C, et al. Geometric analysis of loco-regional recurrences in relation to pre-treatment hypoxia in patients with head and neck cancer. Acta Oncol. 2017; 56: 1571-6.
112. Bluemke E, Bertrand A, Chu KY, Syed N, Murchison AG, Cooke R, et al. Using variable flip angle (VFA) and modified look-locker inversion recovery (MOLLI) T1 mapping in clinical OE-MRI. Magn Reson Imaging. 2022; 89: 92-9.
113. McCabe A, Martin S, Rowe S, Shah J, Morgan PS, Borys D, et al. Oxygen-enhanced MRI assessment of tumour hypoxia in head and neck cancer is feasible and well tolerated in the clinical setting. Eur Radiol Exp. 2024; 8: 27.
114. Featherstone AK, O'Connor JPB, Little RA, Watson Y, Cheung S, Babur M, et al. Data-driven mapping of hypoxia-related tumor heterogeneity using DCE-MRI and OE-MRI. Magn Reson Med. 2018; 79: 2236-45.
115. Heinzmann K, Carter LM, Lewis JS, Aboagye EO. Multiplexed imaging for diagnosis and therapy. Nat Biomed Eng. 2017; 1: 697-713.
116. Katiyar P, Schwenck J, Frauenfeld L, Divine MR, Agrawal V, Kohlhofer U, et al. Quantification of intratumoural heterogeneity in mice and patients via machine-learning models trained on PET-MRI data. Nat Biomed Eng. 2023; 7: 1014-27.
117. Boeke S, Winter RM, Leibfarth S, Krueger MA, Bowden G, Cotton J, et al. Machine learning identifies multi-parametric functional PET/MR imaging cluster to predict radiation resistance in preclinical head and neck cancer models. Eur J Nucl Med Mol Imaging. 2023; 50: 3084-96.

118. Yin SY, Xi RB, Wu AW, Wang S, Li YJ, Wang CB, et al. Patient-derived tumor-like cell clusters for drug testing in cancer therapy. Sci Transl. Med. 2020; 12: eaaz1723.
119. Ren C, Han C. Organoids - preclinical models of human disease. N Engl J Med. 2019; 380: 1981.
120. Bhattacharya S, Calar K, de la Puente P. Mimicking tumor hypoxia and tumor-immune interactions employing three-dimensional in vitro models. J Exp Clin Cancer Res. 2020; 39: 75.
121. Shahpouri M, Adili-Aghdam MA, Mahmudi H, Jaymand M, Amoozgar Z, Akbari M, et al. Prospects for hypoxia-based drug delivery platforms for the elimination of advanced metastatic tumors: From 3D modeling to clinical concepts. J Control Release. 2023; 353: 1002-22.